A MAGNETOTELLURIC STUDY OF SOUTHERN VANCOUVER ISLAND

by

WILFRED NIENABER

B.Sc., University of Victoria, 1969

A THESIS SUBMITTED IN PARTIAL FULFILLMENT

OF THE REQUIREMENTS FOR THE DEGREE OF

MASTER OF SCIENCE

in the Department

of

Physics

We accept this thesis as conforming
to the required standard

[redacted]

UNIVERSITY OF VICTORIA

JUNE 1973

Supervisor: Dr. H.W. Dosso

ABSTRACT

Magnetotelluric studies involve a determination of the electrical subsurface structure of the earth from measurements of the naturally occuring electromagnetic variations at the surface of the earth. In the present work magnetotelluric measurements made at Victoria, B.C. are analyzed. The results are indicative of an anisotropy in the surface impedance with the electric field in approximately the NS direction enhanced by a factor of four or more. The enhancement is possibly due to the effects of discontinuities in the surface layer conductivity at a geological fault, the Leech River Fault, and a seawater channel, the Straits of Juan de Fuca and Georgia, at Victoria.

As is usually the case in anisotropic situations, calculations using the two different orthogonal sets of electric and magnetic field measurements yielded two different results. Often in magnetotelluric work a model of the electrical substructure is proposed on the basis of one set of measurements. In the present work, an interpretative technique employing both sets of measurements is used. The resulting model proposes a highly resistive surface layer followed by a highly conducting layer over a highly resistive earth. The resistivities proposed for the three layers are approximately 4000, 9, and 1000 ohm-m respectively where the first two layers are each 10 km thick.

The validity of the rotational transformation, normally applied to magnetotelluric data in anisotropic situations, is examined experimentally for telluric measurements. A comparison of polarization plots and of power spectra for telluric data transformed into a new coordinate system and for actual measurements in that system only partially verify the form of the transformation. The observed discrepancies may be due to a rather poor quality of signals at certain periods or the possibility that a scalar representation for the conductivity is inadequate.

TABLE OF CONTENTS

LIST OF FIGURES

ACKNOWLEDGEMENTS

I wish to thank my supervisor, Dr. H.W. Dosso for his support and guidance in carrying out the work described in this thesis. I also acknowledge the advice and help of Dr. B. Caner (deceased) in the early stages of this work.

I am grateful to Mr. D. Auld for his assistance with several experimental problems and his advice and suggestions in the analysis of some of the field measurements. For useful discussions and suggestions I am also indebted to Dr. L.K. Law and Dr. E.R. Niblett. I thank also Mrs. C. Benn for her careful typing of this thesis.

Financial support from the National Research Council of Canada through grants to my supervisor is gratefully acknowledged.

CHAPTER 1

INTRODUCTION

1.1 Historical review

The effect of a conductor in the presence of a time varying magnetic field can be described in terms of the electric currents induced within the medium according to the principle of electromagnetic induction. The induced electric field is completely determined by the inducing magnetic field and the electrical structure of the conducting medium. Alternatively, it should be possible to deduce information about the electrical structure of the medium from observations of the fields within the medium. The purpose of magnetotelluric studies is to determine the electrical subsurface structure of the earth from surface measurements of the naturally occuring electromagnetic variations.

The relationship commonly used in magnetotelluric studies involving the electric (E) and magnetic (H) fields at the surface of the medium is derived by solving Maxwell's equations for the appropriate boundary conditions. Since in practice the source intensity is unknown, the solution is conveniently expressed in terms of the ratio of the amplitudes of the orthogonal components of E and H and the phase difference between these components.

Tikhonov (1950), in some of the early studies on the subject of magnetotellurics, realized that the variations in the tangential components

of the electric and magnetic fields at the surface of the earth must be related and demonstrated the relationship for low frequencies. From existing electric and magnetic data for two different geographic locations he calculated the electrical subsurface structure. His calculations were based on the assumption of horizontally uniform fields. Tikhonov and Lipskaya (1952) attempted a more general solution allowing the horizontal gradients of the fields to be finite and recalculated estimates for the structures previously determined by Tikhonov (1950). Lipskaya (1953) presented the electromagnetic equations in a form which clearly described the relationships between the electric and magnetic field components. Later in the same year, Cagniard (1953) presented a definitive analysis of the magnetotelluric method. He outlined a solution for $\underline{E}$ and $\underline{H}$ for a layered earth (N layers) and gave a complete solution for the two-layer case. He also introduced the apparent resistivity as a convenient form containing $|\underline{E} / \underline{H}|$ and outlined a method of interpretation based on the principles of electric and geometric similitude. The method involves the matching of theoretically calculated "master curves" of apparent resistivity (ρ_a) and phase (ϕ) as a function of period or frequency to those calculated from measured values of $\underline{E}$ and $\underline{H}$.

Cagniard's (1953) results were based on the assumptions of uniform source fields and a horizontally uniform earth. These assumptions were challenged by Wait (1954) and Price (1962). Wait (1954) showed that Cagniards (1953) results are valid only if the fields are uniform over a horizontal distance of at least one "skin depth" of the conducting medium.

Price (1962) rederived the field equations for the more general case where the fields need not be uniform and obtained solutions containing a source function with a parameter defined by the source dimensions. He showed that his expressions reduce to those of Cagniard for the appropriate limits of the source terms. Srivastava (1965) used the field equations developed by Price (1962) to derive the apparent resistivity and phase relations for an N-layered medium. In subsequent work Srivastava (1967) applied this solution to two and three-layer models to construct master curves which could be used in the curve matching method proposed by Cagniard (1953).

Magnetotelluric (MT) data have been interpreted with results fairly consistent with other data. Niblett and Sayn-Wittgenstein (1960) used the theory of Cagniard in a modified form to extract information from continuous records of earth potentials at Meanook, Alberta. Cantwell and Madden (1960) applied Cagniard's (1953) theory and interpretation techniques directly to magnetotelluric data at Littleton, Massachusetts.

1.2 Anisotropy

Unfortunately the earth is perhaps better characterized as non-uniform rather than uniform and hence the interpretation of magnetotelluric data is not a simple matter. If each layer of the earth's crust were laterally homogeneous with isotropic electrical conductivity, the ratio of the electric field to the orthogonal magnetic field at some given frequency should be independent of direction. In magnetotelluric studies it is frequently the case that the electric field is enhanced in some particular direction indicating either anisotropic conductivity or a lateral inhomogeneity.

Cases involving anisotropy have been treated by several authors. Srivastava and White (1971), using MT measurements for the east coast of Canada, observed polarization of the electric field which was likely due to the effect of the coastline. Crane and Mainstone (1972) constructed and used a magnetotelluric analogue model to simulate micropulsation field observations near Queensland, Australia and showed that an increase in the amplitude of the electric field was due to the tip of a wedge shaped basaltic structure. Praus et al. (1971) recorded MT measurements and observed telluric polarization at several stations in the Canadian Arctic. A wide distribution in the apparent resistivities at these stations was observed and was attributed to the influence of a highly conducting material at some depth below the surface. Swift (1967) conducted large scale MT observations in the southwestern United States. The data were indicative of anisotropy and were analyzed for tensor apparent resistivities

(the apparent resistivity being dependent on direction). The resulting interpretation showed a highly conducting zone in the upper mantle of the neighbouring region. Reddy and Rankin (1972) attributed the tensor apparent resistivities and telluric polarization in the plains of Alberta to the inhomogeneous structure of the underlying region. Vozoff (1972) used "tensor impedances" as well as a "pseudo-section" technique to interpret MT measurements influenced by conductivity contrasts in southern Texas and the Anadarko basin. (Tensor impedances are related to the $\underline{E}$ / $\underline{H}$ dependence on direction. Psuedo-sections are plots of frequency as a function of horizontal distance for constant apparent resistivities.)

Electromagnetic analogue model studies (Dosso, 1966) demonstrate the effect of a conductivity discontinuity such as a coastline. The model results indicate that for H-polarization of the source field ($\underline{H}$ parallel to the coastline) the electric field is much enhanced as the coast is approached from the landward or highly resistive side reaching a maximum just at the coast while the magnetic field component is little affected. For E-polarization of the source field ($\underline{E}$ parallel to the coastline), this component of the electric field is attenuated, the horizontal magnetic field slightly enhanced, and the vertical component of the magnetic field much enhanced at sufficiently short periods. A deeper lying conductivity contrast than the ocean, such as that of an upwelling in the upper mantle under the sea, produces similar effects at longer periods. Hibbs and Jones (1972) calculated apparent resistivities for two-dimensional models (ones in which the conductivity is a function

of depth and one lateral coordinate) of different lateral conductivity anomalies within the surface of a semi-infinite conducting half-plane. Calculations for various dike widths and the two-layer case where the upper layer has the same conductivity as the dike, showed that for E-polarization the apparent resistivity varies continuously over the dikes while for H-polarization a discontinuity in the apparent resistivity is exhibited at the conductivity discontinuity. It was also noted that for H-polarization and the case where the conductivity of the dike is greater than that of the medium, the apparent resistivity calculated for points over the dike was lower than either of the resistivities. A low apparent resistivity was also obtained for points near a dike of conductivity lower than that of the surrounding medium. The dike also had a significant effect on the H-polarization apparent resistivity curves (ρ_a vs. T). At shorter periods the curves approached those of the two-layer case. However at longer periods the curves approached limiting values in the opposite sense to what would be expected. Consequently, a highly resistive dike over a low resistive medium could be falsely interpreted as a low resistive over a highly resistive layer or vice versa.

Wright (1970) calculated the fields and apparent resistivities for the cases of both E- and H-polarization near a highly conducting graben in the surface layer. The resulting H-polarization apparent resistivity curve had the same shape as the "Cagniard" master curve for the same structure without the graben for all periods but spanned a higher apparent resistivity range. At some distance from the graben the enhance-

ment of the H-polarization curve was less. The E-polarization curve was coincident with the Cagniard curve at longer periods with a notable digression at shorter periods ($T < 500$ sec.). One would expect that at longer periods the effect of the surface and surface anomalies would be less, that $\underline{E} / \underline{H}$ and the apparent resistivity would become less dependent on direction, and, consequently, that the E- and H-polarization curves would approach the same values. However, for all examples shown by Wright (1970), there was no convergence of the E- and H-polarization curves at long periods even though there was no inhomogeneity at depth for his particular models. Thus it seems that a near surface anomaly can cause an apparent resistivity anisotropy which appears over the entire frequency range.

According to Davey and Rosser (1971) the electric fields of geomagnetic micropulsations (Pi 2) can be enhanced by a factor of 4 or more perpendicular to the coastline of a shallow channel of conducting seawater. Caner and Auld (1968) observed a "preferred" direction for the electric field with the electric field in this direction several times greater than in the orthogonal direction for the entire frequency range studied. They, however, reasoned that the electric field measurements of larger amplitudes were realistic while those in the orthogonal direction were distorted by some unknown surface effect. Caner et al. (1969) operated three closely spaced magnetotelluric stations over a known horizontally layered region and found one of the stations to yield anisotropic apparent resistivities. For this station, only the apparent resistivity curve for the lower values

of $\underline{E}$ was in agreement with those of the other two stations and it was deduced that the electric field in the preferred direction was enhanced by some surface distortion of currents. (The region was known to be horizontally stratified from previous Geomagnetic Depth Sounding, a method based on the comparison of variations in the three components of the geomagnetic field recorded at different locations.)

Reddy and Rankin (1970) and Srivastava (1963) proposed methods of interpreting data where the actual resistivity is anisotropic in a given layer. In their methods, information on the ratios of the conductivities in the preferred and orthogonal directions can be obtained from measurements of events with different polarizations of the source field.

1.3 Summary of work in this thesis

In previous magnetotelluric measurements at Victoria (Caner and Auld, 1968), telluric signals were found to be strongly polarized in approximately the NS direction over the entire frequency range. Several arguments were presented to support an interpretation based on data associated with the electric field in the "principal" direction or direction of polarization. More recent results (Caner et al, 1969, Wright, 1970, etc.) tend to favour an interpretation of data for the orthogonal direction. Such an interpretation is employed in this thesis to determine the electrical substructure at Victoria. Results are compared with values previously determined by Geomagnetic Depth Sounding (Caner, 1971). The strong electric polarization at Victoria and its possible causes are also discussed.

When, in magnetotelluric work the data indicate anisotropy, it is necessary before interpretation, to determine the principal direction of telluric polarization and to transform all measurements into a coordinate system with an axis aligned with this direction. The transformation used is also employed in the treatment of tensor apparent resistivities. The form of the transformation, a simple rotation, is known to be valid for magnetic field measurements. In the present work the form is tested for telluric measurements. A selected set of measurements is transformed into a new coordinate system and spectral results in this new system are compared with results of actual measurements in this coordinate system.

CHAPTER 2

MATHEMATICAL ANALYSIS

2.1 Apparent resistivity and phase relations

Much of the vital information about the electrical conductivity distribution in a conducting half-space can be inferred from the ratio of the electric ($\underline{E}$) and magnetic ($\underline{H}$) fields at the surface. The theoretical expression for this ratio was developed by Srivastava (1965, 1967) for an isotropic multi-layered medium using Price's (1962) solution to the wave equation for $\underline{E}$ and $\underline{H}$. Although the theoretical developments by each author are well known, the complete theory will be outlined to provide a unified picture of its development. The theory, as presented here, is the basis of the magnetotelluric interpretation techniques used in this thesis.

Consider a cartesian coordinate system with the origin at the surface of an N-layered half-space (fig. 1). The half-space occupies the region $z > 0$. For a homogeneous, isotropic medium Maxwell's equations (in emu) are:

$$(1) \quad \nabla \times \underline{E} = -\frac{\partial \underline{H}}{\partial t} ,$$

$$(2) \quad \nabla \times \underline{H} = 4\pi \underline{J} ,$$

$$(3) \quad \nabla \cdot \underline{H} = 0 ,$$

where $\underline{J} = \sigma \underline{E}$ is the current density and σ represents the conductivity of the medium. The displacement current is negligible for frequencies

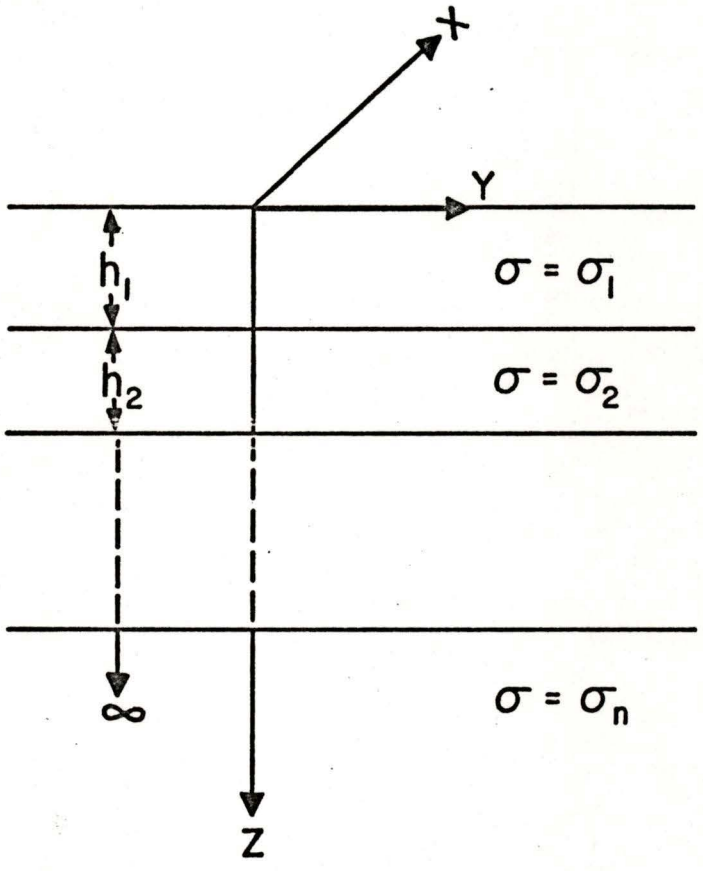

Figure 1. The mathematical model

encountered in magnetotelluric applications . Thus the problem involves the diffusion of the electromagnetic field rather than wave propagation (Price 1962). Taking the curl of equation (1) and assuming the time variation of the fields to be of the form $e^{i\omega t}$, where ω is the angular frequency of variation, leads to

$$(4) \quad \nabla(\nabla\cdot\underline{E}) - \nabla^2\underline{E} = -4\pi i\omega\sigma\underline{E}.$$

The divergence of equation (2) reveals that

$$(5) \quad \nabla\cdot\underline{J} = \sigma(\nabla\cdot\underline{E}) + E_z \frac{d\sigma}{dz} = 0.$$

Price (1950) shows that in a semi-infinite conductor with a plane boundary current flow normal to the surface cannot be affected or produced by electromagnetic induction from outside the conductor. Hence $J_z = 0$, $E_z = 0$ and consequently from (5) $\nabla\cdot\underline{E} = 0$ inside the conductor. Equation (4) now reduces to

$$(6) \quad \nabla^2\underline{E} = 4\pi i\omega\sigma\underline{E}.$$

Price (1962) solves this equation for the electric field.

$$(7) \quad \underline{E} = e^{i\omega t} \; F(z) \left(\frac{\partial P}{\partial y}, \; -\frac{\partial P}{\partial x}, \; 0\right),$$

where P and F are functions satisfying

$$(8) \quad \frac{\partial^2 P}{\partial x^2} + \frac{\partial^2 P}{\partial y^2} + \upsilon^2 P = 0,$$

and

$$(9) \quad \frac{\partial^2 F}{\partial z^2} = (\upsilon^2 + 4\pi i\omega\sigma) \; F,$$

where υ is a constant, with $\frac{2\pi}{\upsilon}$ representing the horizontal scale of the source field. Upon substituting (7) into (1) the magnetic field has the form

$$(10) \quad \underline{H} = \frac{1}{i\omega} \; e^{i\omega t} \left(\frac{dF}{dz} \; \frac{\partial P}{\partial x}, \; \frac{dF}{dz} \; \frac{\partial P}{\partial y}, \; \upsilon^2 FP\right).$$

Srivastava (1965) uses $\underline{E}$ and $\underline{H}$ as given in (7) and (10) to determine the ratio of the electric to magnetic fields in arbitrary layer m of a multilayered medium. In the following analysis the subscript m is used in labelling properties of the m^{th} layer, h_m and σ_m are the thickness and conductivity of this layer. Layers are numbered consecutively from the surface. In the m^{th} layer the solution to equation (9) is

$$(11) \quad F = A_m e^{\theta_m z} + B e^{\theta_m z},$$

where $$\theta_m^2 = \upsilon 2 + 4\pi i \sigma_m \omega,$$

since σ_m is constant within each layer. Using (11) in (7) and (10) and taking the ratio of two orthogonal components Srivastava (1965) obtains

$$(12) \quad \left(\frac{E_x}{H_y}\right)_m = \frac{-i\omega}{\theta_m} \frac{A_m e^{\theta_m z} + B_m e^{-\theta_m z}}{A_m e^{\theta_m z} - B_m e^{-\theta_m z}}$$

$$= \frac{-i\omega}{\theta_m} \coth\left(\theta_m z + \log \left(\frac{A_m}{B_m}\right)^{\frac{1}{2}}\right) .$$

This ratio is commonly referred to as the impedance Z(z) at depth z within the m^{th} layer. The same result can also be obtained by using E_y and H_x (rather than E_y and H_x) and forming the ratio $\left(\frac{-E_y}{H_x}\right)_m$.

The solution for one layer is found by considering m = 1. The subscript is dropped for convenience. Since the constant A must be equal to zero to prevent the fields from becoming infinite as $z \to \infty$, the impedance at the surface of the medium where z = 0 is given by

$$(13) \quad Z(0) = \frac{E_x(0)}{H_y(0)} = \frac{i\omega}{\theta} = \frac{i\omega}{(\upsilon 2 + 4\pi i \sigma)^{\frac{1}{2}}} .$$

Squaring equation (13) and letting $\upsilon \to 0$ to simulate an infinite source field, yields

$$(14) \quad Z(0)^2 = \frac{-\omega^2}{i4\pi\sigma\omega} = \frac{1}{2T\sigma} e^{i\frac{\pi}{2}} ,$$

where $T = 2\pi\omega$ is the period of the variation. The resistivity $\rho = \sigma^{-1}$ of the medium is therefore given by

$$(15) \quad \rho = 2T \left|Z(0)\right|^2 ,$$

and the phase difference between E_x and H_y is $\frac{\pi}{4}$. For geophysical measurements the phase is often different from $\frac{\pi}{4}$ indicating a heterogeneous earth composed of several layers. Let us return to the solution for n layers.

For depths z_a and z_b in the first layer the impedances from equation (12) are

$$(16) \quad Z(z_a) = -\frac{i\omega}{\theta_1} \coth\left(\theta_1 z_a + \log\left(\frac{A_1}{B_1}\right)^{\frac{1}{2}}\right) ,$$

$$(17) \quad Z(z_b) = -\frac{i\omega}{\theta_1} \coth\left(\theta_1 z_b + \log\left(\frac{A_1}{B_1}\right)^{\frac{1}{2}}\right) ,$$

respectively, where $z_a < z_b$. The ratio $\left(\frac{A_1}{B_1}\right)$ can be obtained from (17) and substituted into (16) to yield

$$(18) \quad Z(z_a) = -\frac{i\omega}{\theta_1} \coth\left(\theta_1 (z_a - z_b) - \coth^{-1}\left(Z(z_b)\frac{\theta_1}{i\omega}\right)\right) .$$

Substituting $z_a = 0$ and $z_b = h$, yields the surface impedance in terms of the impedance at the lower boundary of layer 1,

$$(19) \quad Z(0) = -\frac{i\omega}{\theta_1} \coth\left(-\theta_1 h_1 - \coth^{-1}\left(Z(h_1)\frac{\theta_1}{i\omega}\right)\right) .$$

In the same manner, in each layer, the impedance at the upper boundary can be expressed in terms of the impedance at the lower boundary. Since the horizontal fields and the impedances are continuous across the boundary between layers the impedance at the bottom of the $m-1^{th}$ layer is equal to the impedance at the top of the m^{th} layer and we can write

$$(20) \quad Z_{m-1} = -\frac{i\omega}{\theta_m} \coth\left(-\theta_m n_m + \coth^{-1}\left(Z_m \frac{\theta_m}{i\omega}\right)\right),$$

where Z_m denotes the impedance at the lower boundary of the m^{th} layer. Consecutive values of Z_i for n layers are substituted into equation (19) with the result

$$(21) \quad Z(0) = \frac{i\omega}{\theta_1} \coth\left(\theta_1 h_1 + \coth^{-1}\left\{\frac{\theta_1}{\theta_2} \coth\left\{\theta_2 h_2 + \coth^{-1}\left(\frac{\theta_2}{\theta_3} \coth\left(\theta_3 h_3 + \coth^{-1}\frac{\theta_{n-1}}{\theta_n}\right)\right)\right\}\right\}\right).$$

For a three-layer medium the surface impedance is

$$(22) \quad Z(0) = \frac{i\omega}{\theta_1} \coth\left(\theta_1 h_1 + \coth^{-1}\left(\frac{\theta_1}{\theta_2} \coth\left(\theta_2 h_2 + \coth^{-1}\frac{\theta_2}{\theta_3}\right)\right)\right).$$

Srivastava (1967) expresses (22) as

$$(23) \quad Z(0) = \frac{i\omega}{\theta_1} \frac{M + iN}{Q + iR},$$

where M and Q, the real parts, and N and R, the imaginary parts of (22) are given by

$$M = au(cr+p) - bu(dr+q) + s(r+cp-qd) - t(pd+cq),$$

$$N = au(dr+q) + bu(cr+p) + s(pd+cq) + t(r+cp-qd),$$

(24)

$$Q = ru + u(cp-qd) + (as-bt)(cr+p) - (bs+at)(dr+q),$$

$$R = u(cq+pd) + (as-bt)(dr+q) + (bs-at)(cr+p),$$

$$a = (\alpha_1\alpha_2 + \beta_1\beta_2) / (\alpha_2^2 + \beta_2^2),$$

$$b = (\alpha_2\beta_1 - \alpha_1\beta_2) / (\alpha_2^2 + \beta_2^2),$$

$$c = (\alpha_2\alpha_3 + \beta_2\beta_3) / (\alpha_3^2 + \beta_3^2),$$

$$d = (\alpha_3\beta_2 - \alpha_2\beta_3) / (\alpha_3^2 + \beta_3^2),$$

$$p = \tanh \alpha_2\beta_2 \, (1 + \tan^2 \beta_2 h_2),$$

$$q = \tan \beta_2 h_2 \, (1 - \tanh^2 \alpha_2 h_2),$$

$$r = 1 + (\tan^2 \alpha_2 h_2)(\tan^2 \beta_2 h_2),$$

$$s = \tanh \alpha_1 h_1 \, (1 + \tan^2 \beta_1 h_1),$$

$$t = \tan \beta_1 h_1 \, (1 - \tan^2 \alpha_1 h_1),$$

$$u = 1 + (\tanh^2 \alpha_1 h_1)(\tan^2 \beta_1 h_1),$$

$$\alpha_m = 2^{\frac{1}{2}} \left[(k_m^4 + \upsilon^4)^{\frac{1}{2}} + \upsilon^2 \right]^{\frac{1}{2}},$$

$$\beta_m = 2^{\frac{1}{2}} \left[(k_m^4 + \upsilon^4)^{\frac{1}{2}} - \upsilon^2 \right]^{\frac{1}{2}},$$

$$k_m^2 = 4\pi\omega\sigma_m .$$

From (23) the amplitude and phase of the impedance are given by

$$(25) \quad |Z(0)|^2 = \frac{\rho_1}{2T} \, \frac{1}{\frac{(1+\upsilon^4)^{\frac{1}{2}}}{k^4}} \, \frac{M^2 + N^2}{Q^2 + R^2},$$

$$(26) \quad \tan \phi = \frac{\alpha_1 (MQ + NR) - \beta_1 (MR + NQ)}{\alpha_1 (MR + NQ) + \beta_1 (MQ + NR)},$$

where $\rho_m = \frac{1}{\sigma_m}$, and $T = 2\pi/\omega$.

It is obvious that the phase ϕ is the phase difference between $\underline{E}$ and $\underline{H}$.

The "apparent resistivity", ρ_a, defined as

$$(27) \quad \rho a = 2T \left|Z(0)\right|^2$$

is the resistivity of a homogeneous (single layer) formation which would give the same value for the modulus of the ratio of the fields as that observed for the multilayered structure (Cagniard 1953). Using (25), equation (27) becomes

$$(28) \quad \rho a = \rho_1 \frac{1}{(1+\frac{\upsilon^4}{k^4})} \frac{M^2 + N^2}{Q^2 + R^2} .$$

Equations (26) and (28) give the apparent resistivity and phase as a function of the period in terms of the parameters defining the electrical structure of the medium. If the values of the fields are known the impedance can be calculated directly and the apparent resistivity can be obtained from equation (27).

The reason for defining the apparent resistivity as $\rho_a = 2T \left|\frac{E_x}{H_y}\right|^2$ is obvious when one observes its behaviour as a function of the period. It has already been shown that for a homogeneous (1 layer) infinite medium, ρa remains constant since it indicates the actual resistivity of the medium. For a layered medium, in which resistivity varies with depth, ρ_a will vary with the period. Since currents with greater periods penetrate to greater depths, the variation of ρ_a with period must be indicative of the actual resistivity profile. Such electrical information of the structure is inferred by using equations (26), (27), and (28) in a "master curve" technique to be discussed in the next section.

2.2 Interpretative techniques

In a typical magnetotelluric problem the parameters in equations (26) and (28) (or similar equations for the appropriate number of layers) are not known. The apparent resistivity curve (ρ_a as a function of period) which reflects the subsurface structure of the earth is calculated from equation (27) using experimentally measured values of the electric and magnetic fields. The phase curve (ϕ as a function of period) is plotted directly from measured values. The entire magnetotelluric sounding is represented by these two curves. The data in this form are "inverted" to yield the structure parameters by matching to curves of the form of (26) and (28) for 2, 3, or 4 layers.

A method of interpreting a two-layer structure was suggested by Cagniard (1953). A limited number of master curves are constructed using different values for the parameters in the apparent resistivity and phase relations. Both the master curves and the experimental curves are plotted on logarithmic graph paper and the experimental curves are matched to master curves of the same shape. Cagniard uses the laws of electric similitude to show that some parameters can be deduced from the vertical and horizontal shifts between the experimental and master curves while others can be inferred from the ratios of certain parameters of both curves. An expansion of this method which would yield approximate solutions for three or more layers was also proposed by Cagniard (1953).

Srivastava (1967) provided a set of master curves based on equations (26) and (28) and suggested utilizing them in a manner similar

to that of Cagniard with only a slight modification to accomodate the source parameter υ.

The technique most conveniently suited to the work in this thesis involved the use of Srivastava's (1967) equations in computer program form to recalculate master curves for varying parameters and select the best fitting model.

In cases where the surface impedance $|\underline{E} / \underline{H}|$ is not independent of direction the interpretation becomes more complex. Several techniques have been used. For the case of two-dimensional models involving a vertical fault, Weaver (1963) showed that the entire theoretical problem can be represented by two independent cases; E-polarization where the electric vector is parallel to the fault, and H-polarization where the magnetic vector is parallel to the fault. Since it is well known that the electric field perpendicular to the fault is much enhanced it is only necessary to determine the major and minor axes of the electric polarization ellipse and transform all measurements into a coordinate system with axes aligned in these directions. The apparent resistivity and phase curves calculated from orthogonal sets of $\underline{E}$ and $\underline{H}$ from these data are then those of the E- and H-polarization cases. The interpretation is carried out on these sets of curves.

An alternative method involves the calculation of the elements of the impedance tensor satisfying $\underline{E} = \underline{\underline{T}}\,\underline{H}$ (Swift 1967, Vozoff 1972). A rotational transformation is applied to the complete impedance tensor to

minimize the diagonal elements. The resulting off-diagonal elements furnish information similar to that of the E- and H-polarization apparent resistivities of the former method.

CHAPTER 3

EXPERIMENT

3.1 Methods and instrumentation

Two telluric systems were set up on a remote area of the grounds of the University of Victoria. The two coordinate systems used, the magnetic NS-EW system, referred to as the "primary system", and the "offset" system, at an angle of 25^{o} clockwise with respect to the primary system, are shown in figure 2.

Electrodes for the telluric measurements consisted of lead plates 0.0032 m thick and 0.61 m square (1/8 in. x 2 ft. x 2 ft.) buried at a depth of 1.83 m (6 ft.). The separation between electrode pairs for both systems was 91.4 m (300 ft.) with the resistance between electrodes of the order of 150 ohms.

In the primary system both horizontal components of the electric and magnetic fields were recorded simultaneously. Electric field measurements in the offset system provided data for testing the rotational transformation. In order to record variations over a very wide frequency band and still retain reasonable accuracy the recording was done in two sections; short-period (20-500 seconds) and long-period (400 seconds — d.c.). The recording equipment and frequency response curves are shown in figure 3. During the several month period when simultaneous recording of both telluric systems took place, the Neff amplifiers, since only two

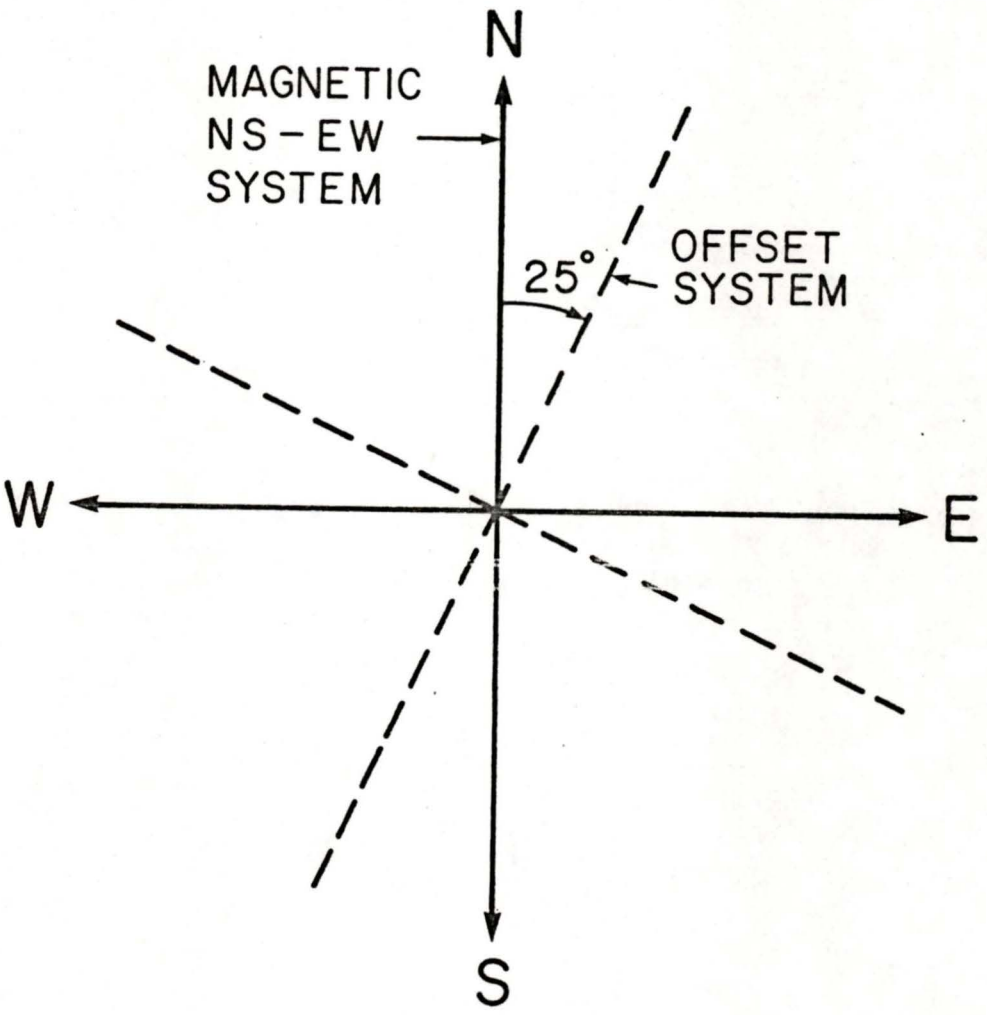

Figure 2. Telluric coordinate systems

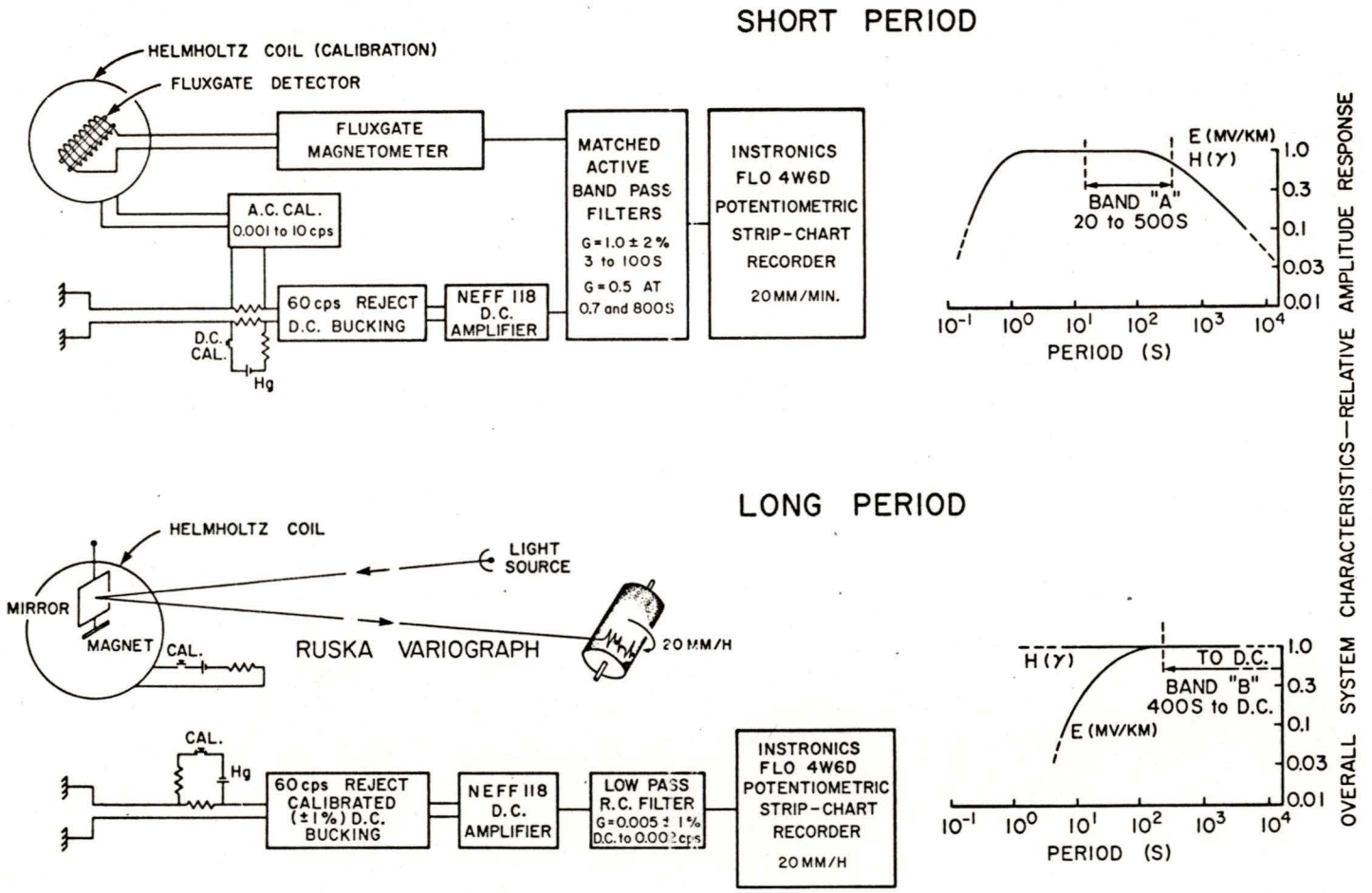

Figure 3. Instrumentation and frequency response

were available, were replaced by four Medistor amplifiers (type A-61RB modified). The four Medistor amplifiers kept the four channels closely matched, eliminating the need for frequency response corrections.

For the telluric measurements the same electrodes and amplifiers were used for recording in both period ranges with only a change in the filtering network. However, for the magnetic field measurements two different monitoring systems were used. The short-period magnetic variations were recorded using a saturable core fluxgate magnetometer (Trigg et al., 1971) located at the telluric station site. Signals were passed through the same type of filtering network and into the same strip chart recorder as the telluric signals. The long-period magnetic variations were recorded at the Victoria Geophysical Observatory (15 km distance from the telluric station site) using a Ruska photographic variometer. Long-period magnetograms are produced daily as part of the function of the observatory. These magnetograms were assumed to be representative of the long-period variations at the university site since geomagnetic variations at these periods are consistent over such relatively short distances as 15 km if there are no large conductivity contrasts between the two stations.

Calibration of the telluric recording system was achieved by injecting signals of known amplitude in series with the electrode cables (see figure 3). A Sprengnether TS 100 model 438B chronometer with a relay in parallel with the calibration switch on the amplifier was used to initiate the calibration time marks on the telluric traces. The

magnetic recording system was calibrated with the aid of a known magnetic field provided by a Helmholtz coil.

3.2 Data processing and interpretation

Short-period data

Sections of telluric and magnetic record tracings approximately 44 minutes long were digitized at an interval of 1/3 mm. corresponding to one second (N = 2667 points). Longer sections would perhaps produce better spectral results at the long periods but chart lengths were limited by the size of the digitizing drum. An example of one section of short-period data is shown in figure 4. Power spectral analysis was carried out with 200 lags on the data (Blackman and Tukey, 1958). A listing of the computer program appears in appendix A. Apparent resistivity, phase, and coherence between telluric and magnetic variations as a function of period were calculated using auto and cross-correlation techniques. Resulting values of apparent resistivity and phase were accepted only if the coherence value exceeded 0.75. Values of apparent resistivity and phase for cases where the coherence was 0.95 or greater were weighted by a factor of three when used in the construction of apparent resistivity and phase curves.

Long-period data

Selected sections of telluric and magnetic record varying in length from 24 to 29 hours were digitized at an interval of ¼ mm. corresponding to 80 samples per hour. A representative long-period section appears in figure 5. Chart lengths were limited by the short duration of significant magnetic activity. Again power spectral analysis was carried

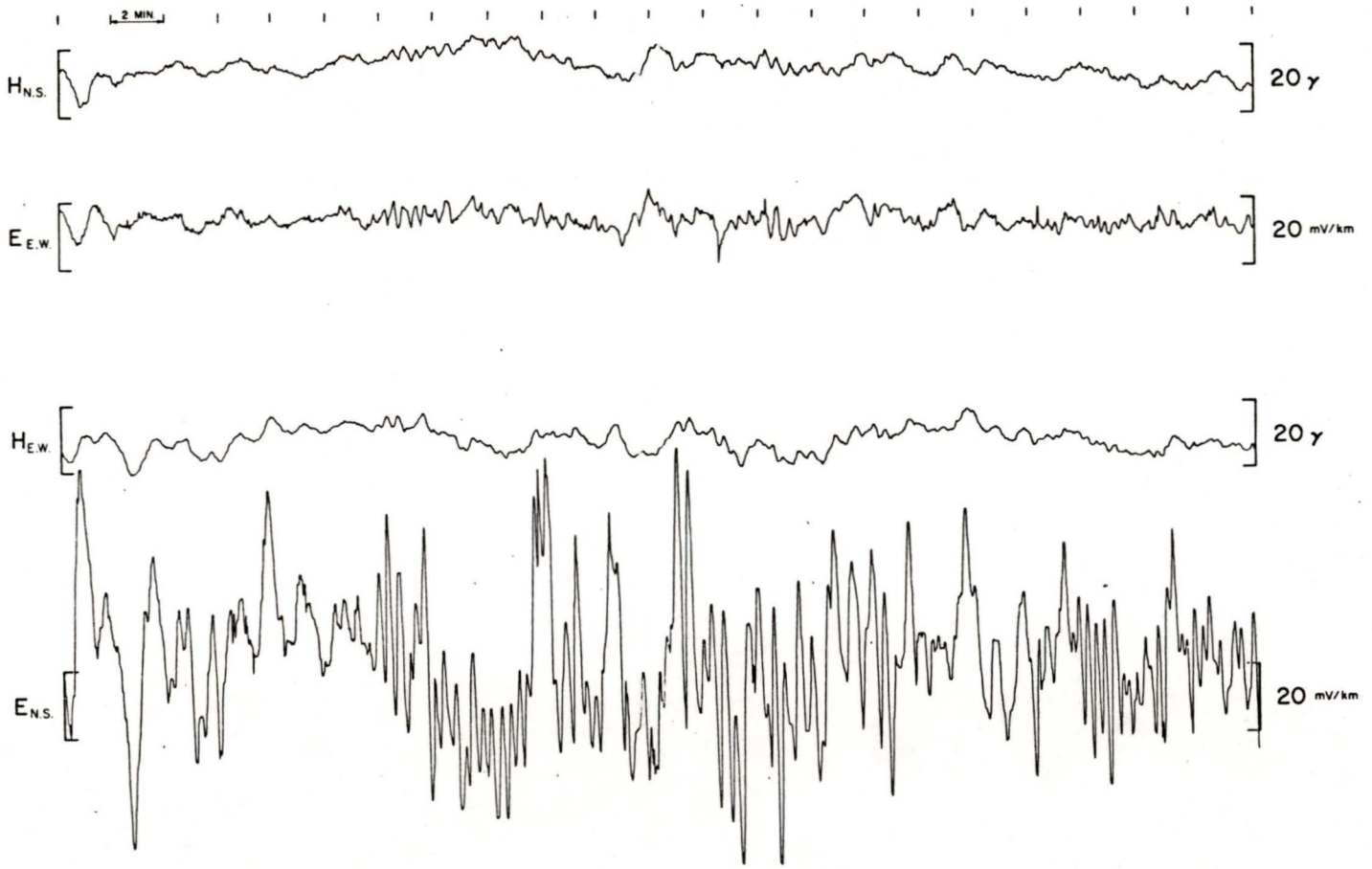

Figure 4. Section of short-period magnetotelluric record taken at the University of Victoria (May 30, 1971, 1500 U.T.)

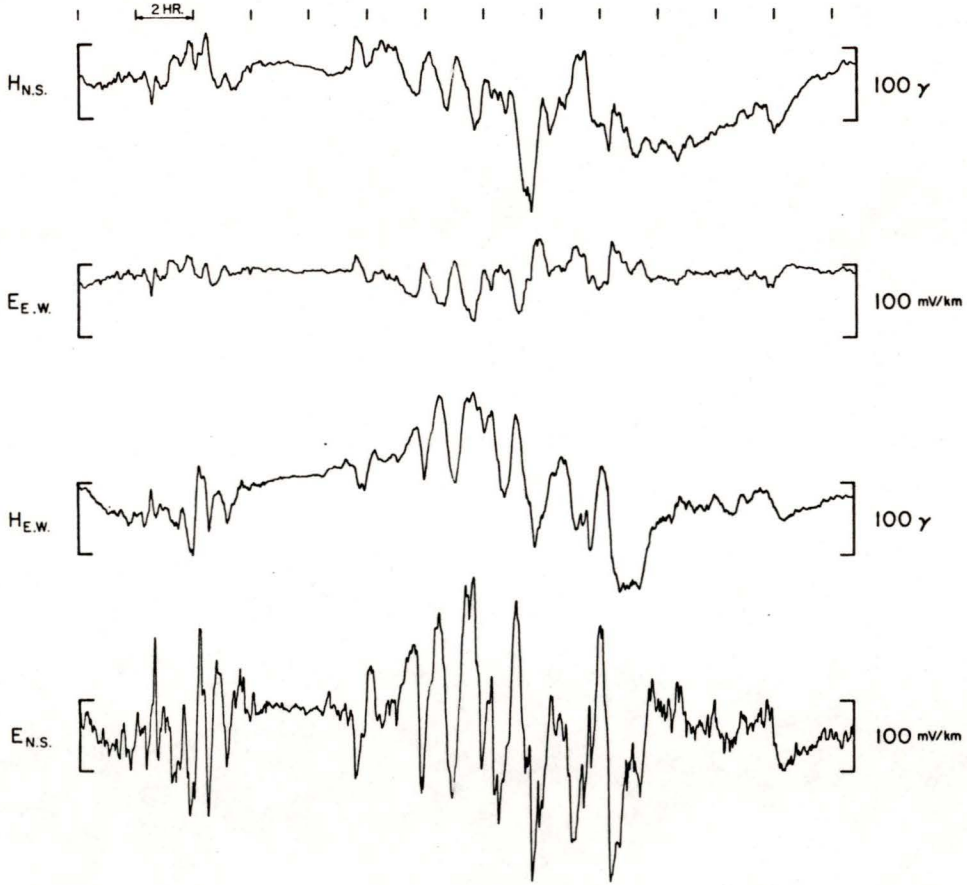

Figure 5. Section of long-period magnetotelluric record taken at the University of Victoria (Feb. 10, 1969, 2100 U.T.)

out with 200 lags on the data and apparent resistivities and phase calculated with the same criterion for acceptable values as was used for the short-period analysis.

Apparent resistivity and phase values were calculated only for periods up to three hours in length. On the basis of work by Caner and Auld (1968) it was assumed that there was no tidal contribution to the telluric data at the periods considered in the present work. Their results indicated that there is no significant tidal energy present for periods less than 8 hours.

Apparent resistivity and phase were calculated for both sets of orthogonal components E_{NS}/H_{EW} and E_{EW}/H_{NS}. In cases where the apparent resistivities for these two sets are not the same the most meaningful results are those related to the principal directions of the apparent resistivity anisotropy (directions of maximum and minimum apparent resistivity which are also related to the H- and E-polarization cases of the two-dimensional fault problem). Therefore it is necessary to transform, before power spectral analysis, the field measurements into a coordinate system whose axes represent the principal directions. The principal directions are found by determining the major and minor axes of a polarization ellipse of the electric field. Only events for which the magnetic field is circularly polarized (see figure 6) are chosen so that the ellipsi indicate only the "inherent" polarization or polarization due to the geological structure. It will be seen in the next section that the principal directions of telluric polarization were rather closely aligned with the NS-EW

coordinate system in which the field measurements were made. A transformation of the data was not required since it would have involved only a rotation of approximately three degrees.

CHAPTER 4

DISCUSSION OF RESULTS

4.1 Polarization

The telluric signals at Victoria were found to be strongly polarized, the NS component being several times larger than the EW component, over the entire frequency range. This effect can be observed from the actual traces in figures 4 and 5 since the amplitudes of both magnetic components are approximately the same.

The direction of polarization, or the direction in which $\underline{E}$ experiences the maximum enhancement, can be determined by plotting the electric field vectors over a period of time when the magnetic variation is circularly polarized. Examples of such polarization plots (hodographs) for both period ranges are shown in figure 6. The major axis of the electric polarization ellipse defines the direction of polarization. At Victoria the direction of the telluric polarization averaged for two long period (60-80 min.) and two short period (115-150 sec.) events was approximately 3 degrees east of magnetic north.

There are several possible causes of this direction of polarization. Three, in particular, are associated with a two-dimensional model. Strikes of highly conducting bodies such as the coastline and a fault at Victoria are shown in figure 7. Firstly, the coast effect is an aspect to be examined. The shortest distance to the continental slope from Victoria

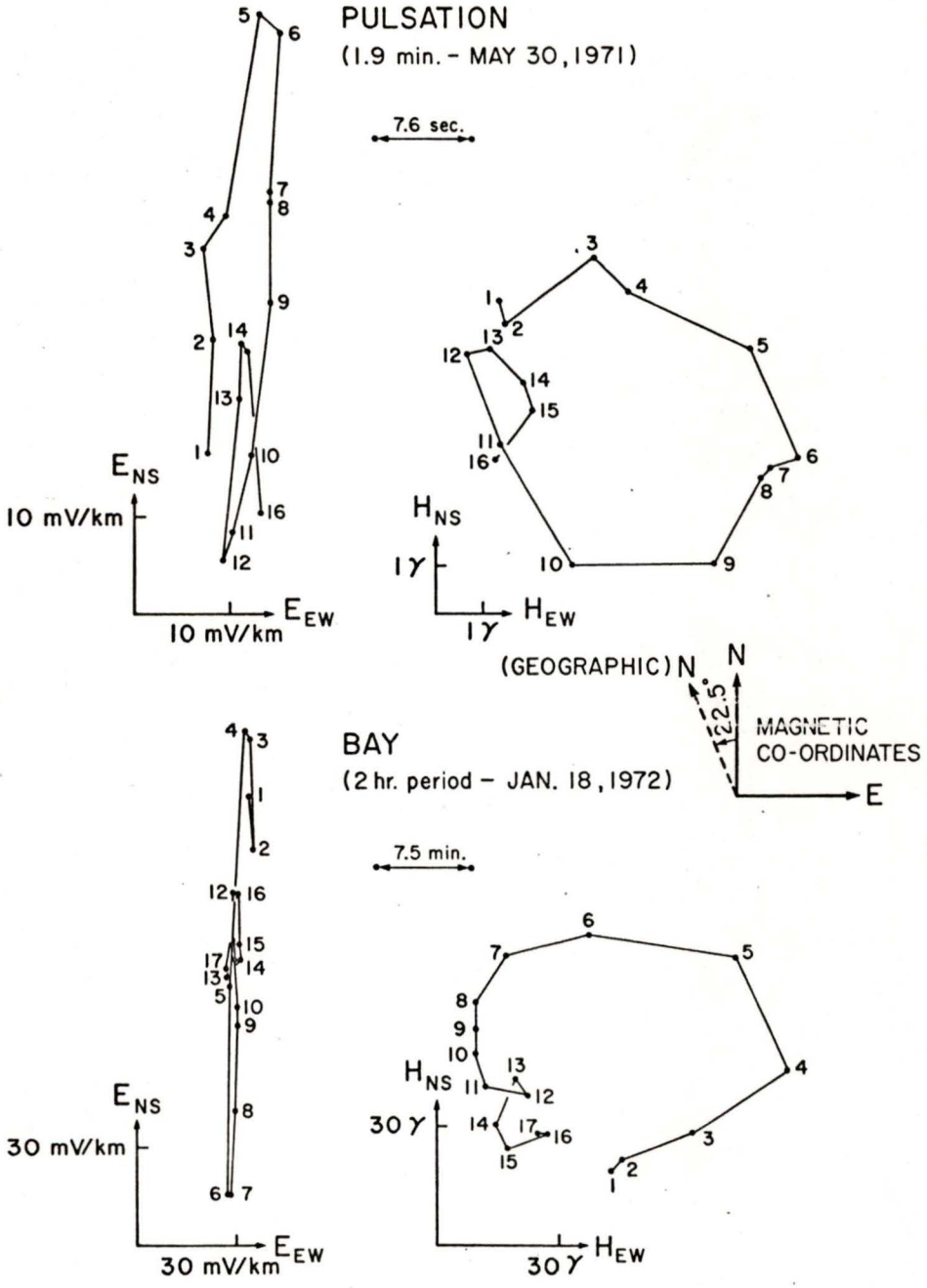

Figure 6. Polarization diagrams

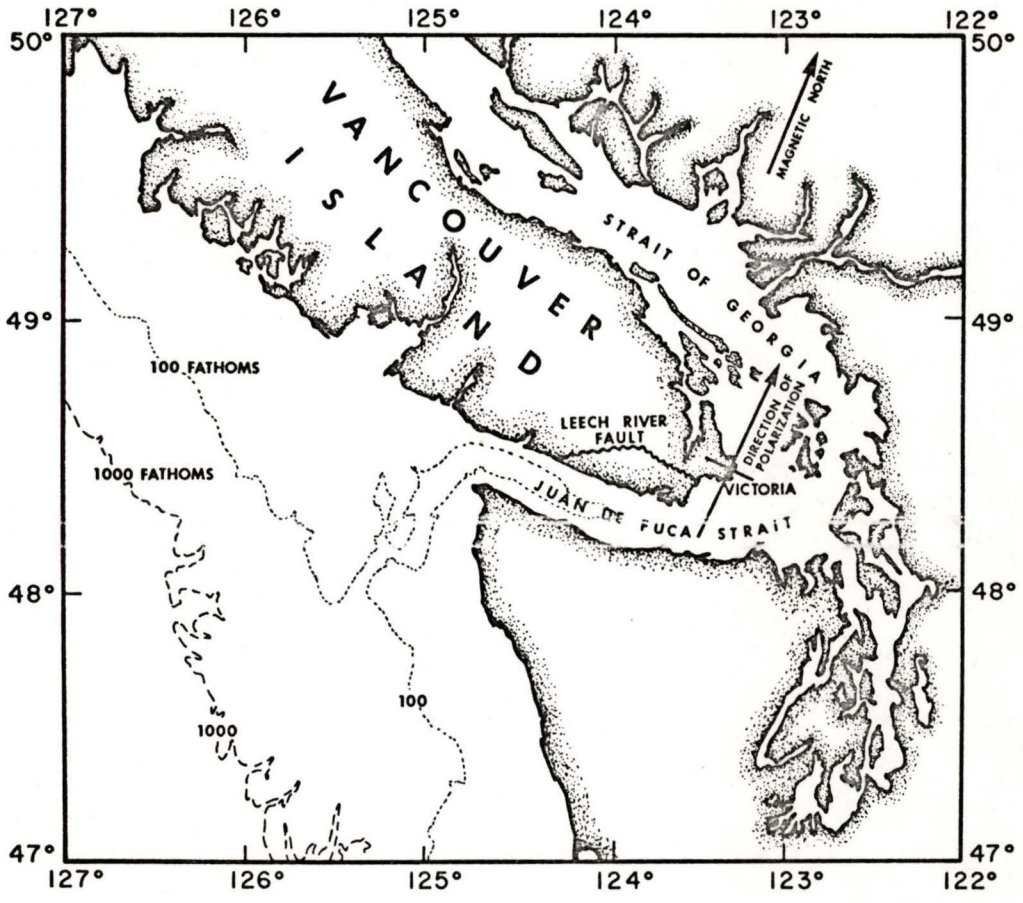

Figure 7. Relative orientations of polarization direction, the coast, and the Leech River Fault on southern Vancouver Island

is approximately 150 km while the distance to the deep ocean is of the order of 220 km. According to Dosso (1966) the coast effect is unimportant at these distances as far as the electric field is concerned. Further, Wescott (1967) showed that while the enhancement of the electric field component perpendicular to the coast was readily observed for stations within 15 km of the Alaskan coast, it had disappeared for a station 45 km inland. Also, assuming that the 100 fathom line indicates the direction of the shelf near Victoria, there is a discrepancy of 20 to 25 degrees between the vector normal to the general contour of the continental shelf and the direction of polarization. These factors would indicate that the enhancement at Victoria is probably not related to the proximity of the Pacific continental shelf or deep ocean. An upwelling in the upper mantle structure under the ocean as modelled by Dosso (1966) may cause telluric polarization at Victoria providing the upwelling begins at a considerable distance to the landward side of the continental slope (i.e. closer to Victoria). However such a structure would be expected to produce a Geomagnetic Depth Sounding anomaly of which there is no evidence at Victoria. Secondly, even though the polarization may not be directly related to the deep ocean, it must be remembered that the channel at Victoria is attached to the large ocean forming a closed branch loop of that ocean. Hence currents induced in the deep ocean could have branch currents flowing in the channel. Such an effect was proposed by Edwards et al. (1971) in analyzing a Parkinson survey of the British Isles. The vectors for very long periods pointed to the deep ocean, while those for more intermediate

periods pointed to the shallow seas even though currents induced in the shallow seas alone were insufficient to produce them. Transfer function arrows at Victoria (Cochrane and Hyndman, 1970) display approximately the same behavior. If the branch currents do exist in the channel at Victoria they would have some effect on the magnetic transfer function and the electric polarization direction. The effect is difficult to assess since the direction of the coastline at Victoria and the direction to the sea-water channel is ill defined. Victoria is situated at the tip of Vancouver Island with a very irregular coastline and many nearby small islands.

The possibility that the Strait of Juan de Fuca and/or the Strait of Georgia, without considering the deep ocean, are possible causes of the observed polarization needs to be examined. Polarization at the short periods could readily be affected by a shallow channel. Davey et al. (1971) found the English Channel to enhance the horizontal electric field (4-5 times) for periods up to 100 seconds. The effect of shallow conducting bodies need not be limited to the short periods. Caner et al. (1969) observed an electric enhancement at an inland station for the entire period range studied ($1\text{-}10^4$ sec.). The effect was attributed to a near surface distortion of telluric currents since the measurements were made in a region where the substructure was known to be horizontally stratified. Calculations of apparent resistivity near a shallow conducting graben by Wright (1970) produced apparent resistivity curves which were enhanced over the entire MT period range ($1\text{-}10^4$ sec.) for H-polarization of the source field. On the basis of these results, polarization of the electric field

due to the shallow channel at Victoria can be considered possible. As in the case of branch currents, the effect is difficult to assess due to the irregular nature of the coastline.

A geological feature known as the Leech River Fault may also affect the telluric polarization. The fault separates the southern tip of Vancouver Island into two regions of different crustal compositions; Eocene (Metchosin volcanics) to the south of the fault and Paleozoic and Lower Mesozoic intrusives to the north (Geological map, Muller, 1971). The known extent and strike of this fault are shown in figure 7. The fault may well extend across the strait as the crustal composition of the mainland to the south of Vancouver Island is also predominantly Eocene volcanics. Since the Mesozoic intrusions are more resistive than Eocene volcanics by a factor of two or more (2-15) (Samson, 1959) a conductive interface exists along the fault plane with the station at Victoria on the more resistive side. If the fault extends across the Strait of Georgia it could have an important effect on the polarization. This effect may be more important than the coast effect since the observed direction of polarization is perpendicular to a straight line extension of the fault across the strait.

4.2 Apparent Resistivity Curves

The experimental values of apparent resistivity and phase as a function of period from power spectral analysis results when plotted showed considerable scatter. The results of averaging these apparent resistivity values over equally divided bandwidths and the standard deviation for each band are shown in figure 8. The phase data are omitted from the discussion as the scatter was too great to delineate any useful curves.

In figure 8 values of apparent resistivity for both sets of orthogonal components are shown. The almost uniform separation of the two curves is a direct result of the polarization. The parallel nature, much like that of Wright's (1970) curves, strongly suggests the existence of a near surface anomaly producing a fairly high conductivity contrast. The solid heavy lines in figure 9 show the statistical limits defined by the standard deviations in apparent resistivity. The dashed sections indicate regions where the standard deviations vary widely from point to point.

Model curves for different conductivity structures using the techniques developed by Srivastava (1965, 1967) were fitted to the statistical limits. The thin solid and dashed lines represent curves for an infinite source field or "Cagniard curves" while the dotted lines show the effect of a source field of finite dimensions. The E_{NS}/H_{EW} and the E_{EW}/H_{NS} curves are often referred to as the major and minor axis curves respectively since they correspond to measurements of the electric field

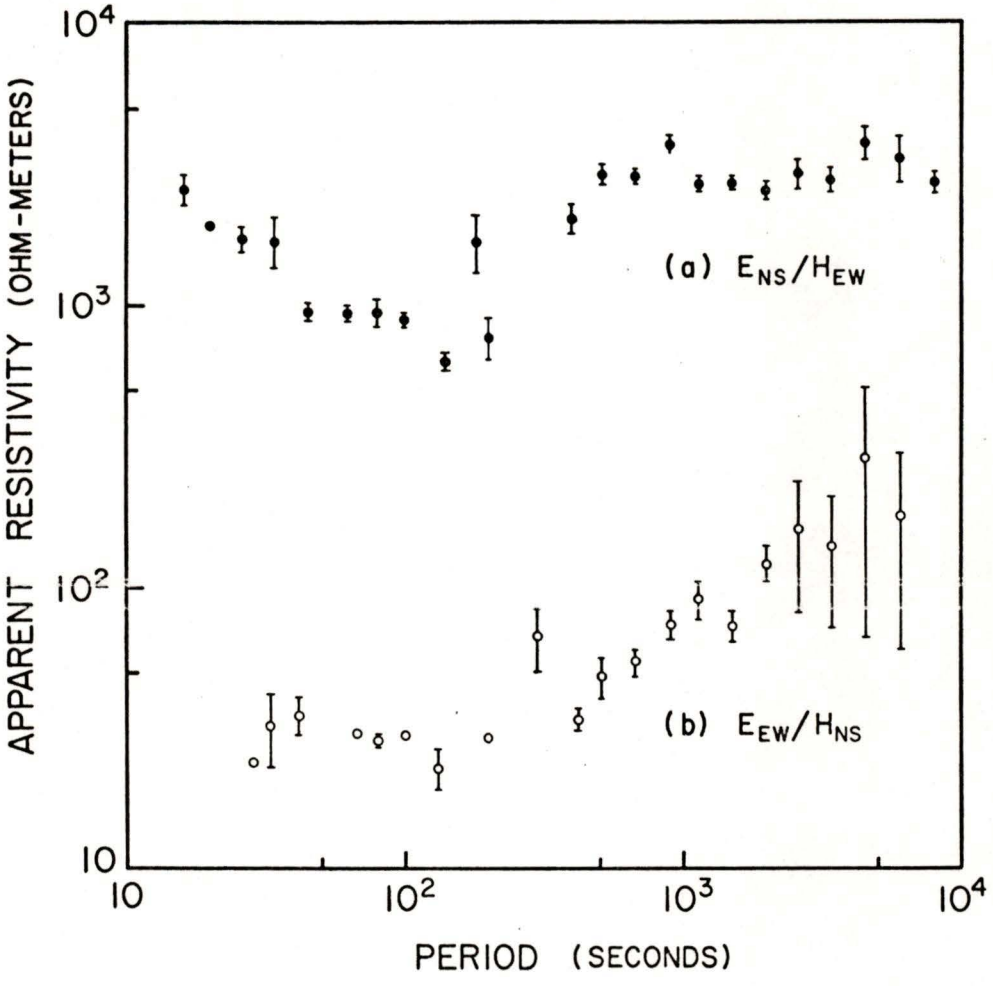

Figure 8. Average values and standard deviations of apparent resistivity as a function of period for equally divided bandwidths

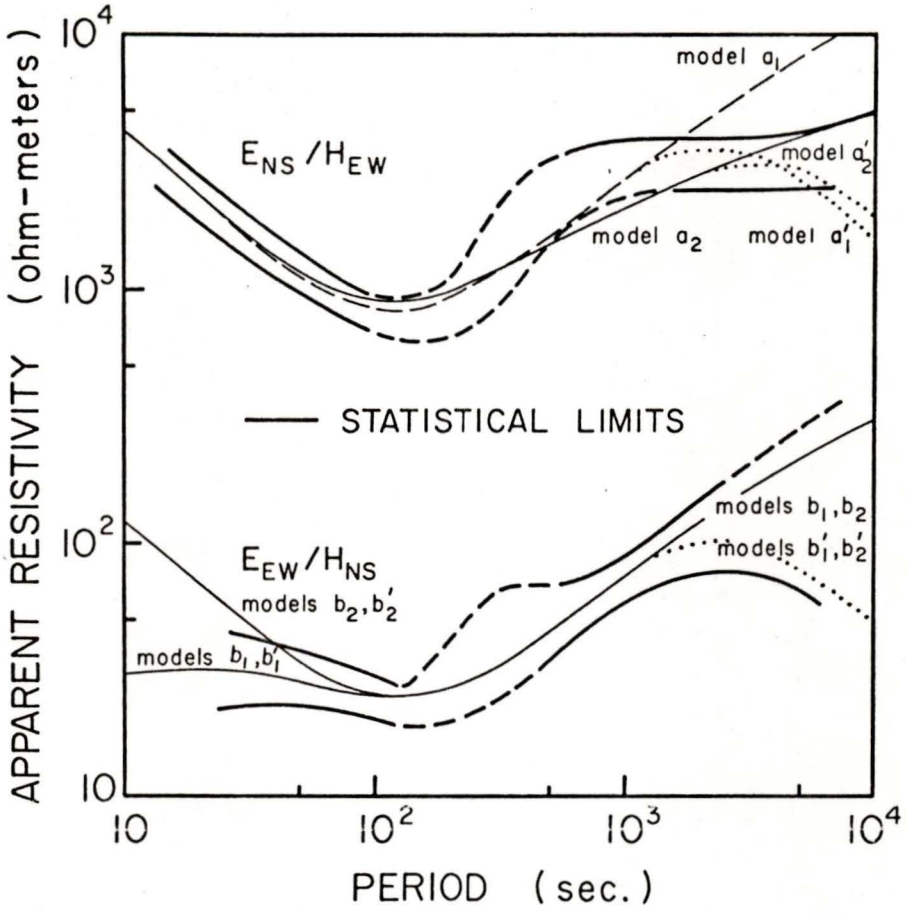

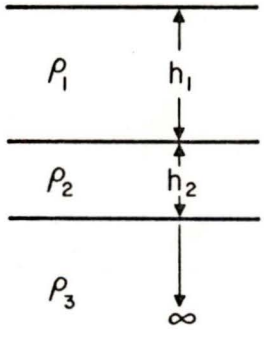

MODEL	ν_L (km^{-1})	h_1 (km)	h_2 (km)	ρ_1 (Ωm)	ρ_2 (Ωm)	ρ_3 (Ωm)
a_1	0.0	75	9	6000	51	4×10^4
a_1'	.0007	75	9	6000	50	4×10^4
a_2	0.0	75	7.5	6000	50	8000
a_2'	.0006	75	7.5	6000	49	8000
b_1	0.0	25	5	30	15	1000
b_1'	.004	25	5	30	14	1000
b_2	0.0	10	10	4000	9	1000
b_2'	.004	10	10	4000	8.5	1000
CANER'71		10-15	20-40		~ 5	30-75

Figure 9. Model curves fitted to statistical limits of experimental data. Limit curves are dashed where the standard deviations vary widely from point to point.

in the directions of the major and minor axes of the telluric polarization ellipse. These curves are also the E- and H-polarization curves. Models a_1 and a_1' fit the E_{NS}/H_{EW} data well. However the structure represented by these curves ascribes an unrealistically high value to the upper mantle resistivity. Models a_2 and a_2' provide a more realistic fit. Models b_1 and b_1' provide the best "Cagniard" and finite source fits respectively to the E_{EW}/H_{NS} data. Model curves b_2 and b_2' have been constructed parallel to a_1 in the short period range.

Recently there has been some controversy over which set of data, major or minor axis data, yields the most realistic interpretation. Model a_2 is in close agreement with previous results determined by Caner and Auld (1968) for the Victoria area. An argument in favour of modelling from the upper, or major axis curve, (Caner and Auld 1968) was based on a strong correlation between E_{NS} and H_{EW} with considerably poorer correlation between E_{EW} and H_{NS}. Furthermore the power spectrum of E_{EW} merely followed that of E_{NS}. For the present measurements, however, the correlation between E_{EW} and H_{NS} is reasonably high with E_{EW} having a power spectrum significantly independent of E_{NS}. Moreover, if the electric field is enhanced in the NS direction it is no longer reasonable to base a model on this component of the electric field. The enhanced nature of the H-polarization curve with respect to the Cagniard curve for the one-dimensional structure has been demonstrated by Wright (1970) and Hibbs and Jones (1971).

The minor axis curves (b_1 and b_1') yield a more realistic model

of the conductivity structure than the major axis curves. The electric field associated with the minor axis data (E parallel to the strike of a highly conducting body) is affected only at very short periods and at very short distances from the edge of the highly conducting body (Dosso, 1966). Wright (1970) showed that the E-polarization apparent resistivity curve should approximate the Cagniard curve for sufficiently long periods. Experimentally, Caner et al. (1969), in working with the three station cluster over a horizontally stratified region, found that only the lower or minor axis curve of the anisotropic station yielded a model which agreed with that of the other two stations.

A possible refinement to choosing the minor axis apparent resistivity curve alone for modelling was implicitly suggested by Wright (1970). Apparent resistivities calculated for stations near the highly conducting surface graben showed that the E-polarization curve at longer periods was coincident with the Cagniard curve. However at shorter periods this was no longer the case. On the other hand the H-polarization curve was not coincident with the Cagniard curve but roughly parallel to it for the entire period range. Therefore, using the suggestion of Wright (1970) that both the E- and H-polarization curves be combined into one interpretation, model curves b_2 and b_2' of figure 9 were constructed using the EW data in the long period range and a segment parallel to the NS data, or model curve a_1, in the short period range. The end result of this technique was a model derived from an apparent resistivity curve approximately parallel to the major axis apparent resistivity curve but in the

resistivity range of the minor axis curve.

The technique of using the major as well as the minor axis measurements has the advantage of an improved signal to noise ratio due to an enhanced signal. The value of the major axis data is well illustrated by the data of the present work since the coherences between magnetic and telluric signals is generally higher for the E_{NS} data than the E_{EW} data.

The results in figure 9 indicate a considerable difference between model b_2 (obtained using both major and minor axis apparent resistivity curves) and model b_1 (obtained using the minor axis apparent resistivity curve only). Model b_1 yields an extremely low rather than high value of the resistivity of the first layer. Also, if there is to be even a slight inflection in curve b_1 at approximately 40 seconds as the data would indicate, then a large value for the thickness of the first layer is required as well as a very small value for the second layer thickness. It should be noted that for the short-period section the values for curve b_1 are essentially established once a value for ρ_1 has been chosen.

On the basis of previous geological data and the model proposed by Caner (1971) for the "low Z" region of British Columbia (extending from the Rocky Mountain Trench to the Pacific coast) figure 9 indicates that model b_2 is much preferred over b_1. The surface resistivity, although not given for the model of Caner (1971), is known to be very high ($\sim$2000Ωm) (Muller 1971, Samson 1969), a value much closer to that of b_2 than that of b_1 .

The dotted lines in figure 9, labeled with primed symbols, illustrate the effect of finite source parameters on the model curves. Model curves with values of υ_L in the range 0-.004km^{-1} ($\infty \geq$ wavelength $\geq$ 1570km) can be fitted to the data. According to Price (1962) values of υ_L from 1.57×10^{-4} to 1.57×10^{-2} km^{-1} (40,000 km $\geq \lambda \geq$ 400km) are reasonable. (40,000 km $\simeq$ circumference of the earth and 400 km $\simeq$ 4 x the height of ionospheric currents).

The deviation of the apparent resistivity for finite sources from the Cagniard curves is most pronounced at very long periods. It is also noted that for the E_{EW}/H_{NS} curve the statistical limits diverge at these same long periods allowing apparent resistivity curves for several values of υ_L to be fitted to the data. The upper and lower statistical limits of these data have the forms of curves for which $\upsilon_L = 0$ and $\upsilon_L = .004$ km^{-1} respectively. This effect could be interpreted as a change or many changes in the source dimensions while measurements of the electric and magnetic fields were being made.

The dotted lines in figure 9 are fitted to a possible inflection in the data at long periods. If this inflection is real it need not only be attributed to a source effect but may also be an indication of another conducting layer.

It is concluded that model b_2 depicts the most realistic subsurface conductivity structure at Victoria. This model proposes a highly conducting layer 10 km thick embedded in a highly resistive earth 10 km from the surface. Model curve b_2 indicates that during the course of measurement typical source dimensions may have been as small as 1570 km.

4.3 Rotation of telluric axes

In the treatment of polarized telluric data it is necessary to transform data from the magnetic NS-EW coordinate system into a coordinate system with axes in the principal directions associated with the polarization. Either the original data are transformed directly or the impedance tensor in the NS-EW system is operated upon by a transformation matrix (Swift, 1967). Both transformations involve a simple vector rotation. It was therefore proposed to attempt an experimental check of the validity of this form of transformation for telluric measurements. An obvious method is to derive the principal directions of the polarization from the magnetic NS-EW orientation data, install new electrode pairs along the derived major and minor axes and record in both coordinate systems. Rather fortuitously, the magnetic NS axis very nearly coincided with the major axis ($\sim 3^{o}$) for the present measurements. Therefore the NS-EW coordinate system was designated as the principal axis coordinate system and an offset was created with axes rotated 25^{o} clockwise with respect to the principal axes.

In both the long and short-period bands, data in the two coordinate systems were obtained simultaneously. Sample tracings are shown in figures 10 and 11. After digitizing, the data from the offset system were computationally rotated into the principal coordinate system using a transformation of the form

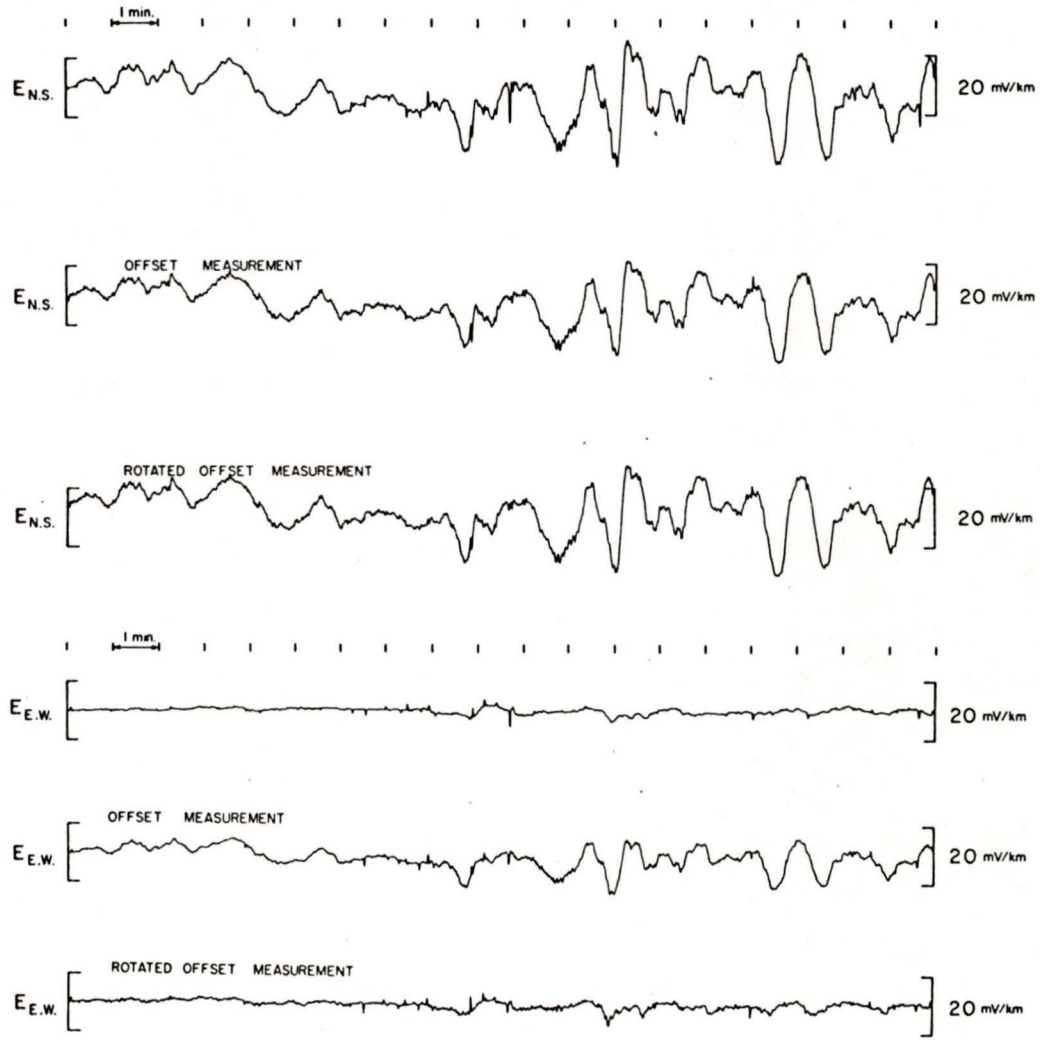

Figure 10. Section of short-period magnetotelluric record for the two telluric systems at Victoria (Apr. 19, 1972, 1141 U.T.). Transformed (rotated) measurements are also shown.

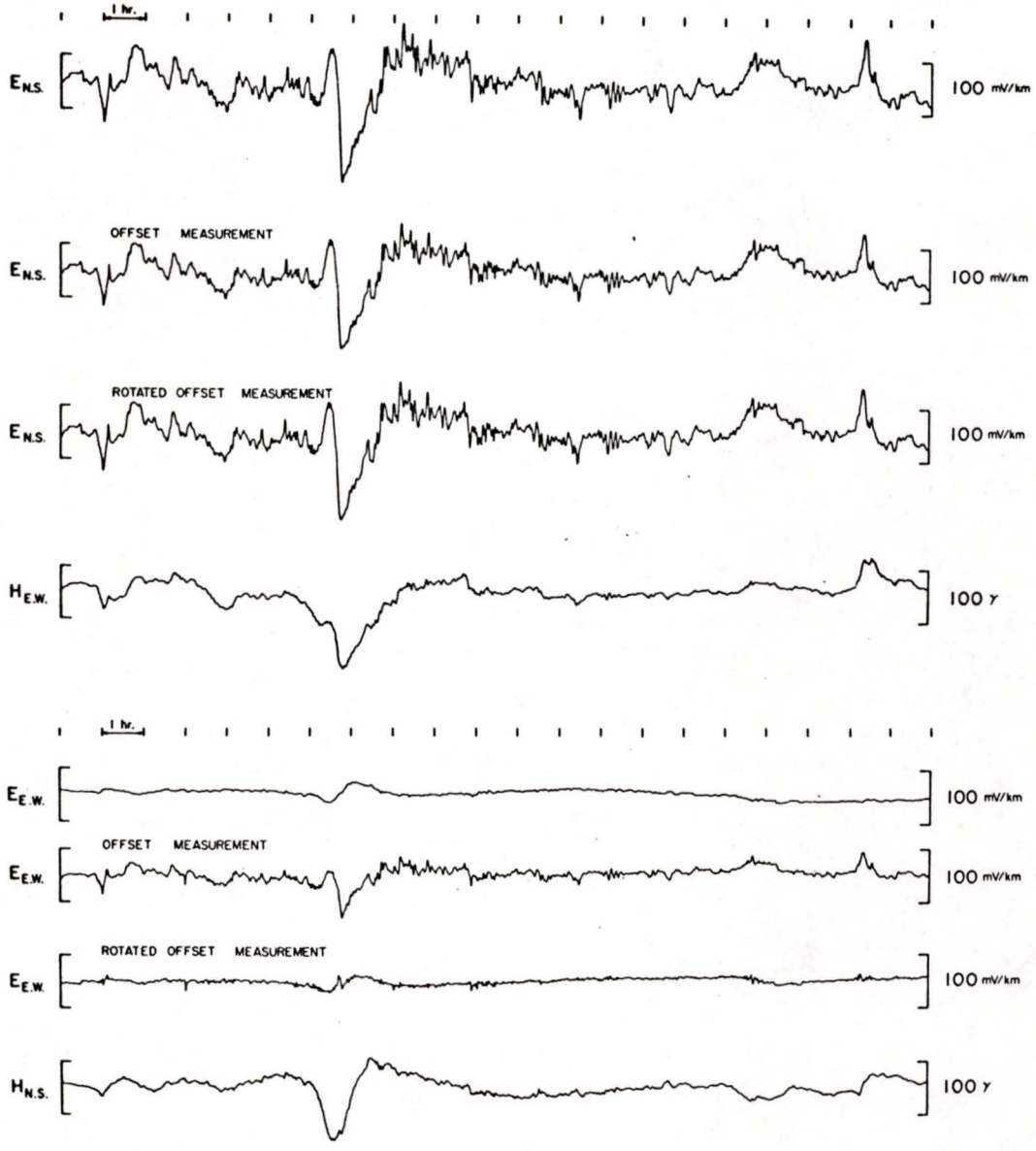

Figure 11. Section of long-period magnetotelluric record for the two telluric systems at Victoria (Jan. 16, 1972, 0900 U.T.) Transformed (rotated) measurements are also shown.

$$E_{NS} = E_{NS} \cos\psi + E_{EW} \sin\psi,$$

$$E_{EW} = E_{EW} \cos\psi - E_{NS} \sin\psi,$$

where ψ is the angle through which the axes are to be rotated.

Figure 12 shows polarization plots (short and long-period) for measurements in both coordinate systems. The angles between the major axes of each pair of ellipsi are shown. From these angles it would appear that the two coordinate systems are separated by a rotation of approximately 27^{o}. Hence a rotation of 25^{o} applied to the offset system measurements yielded results similar to those of the principal axes system. Comparing the lengths of the major and minor axes of each pair of plots shows that differences between the amplitudes of E_{NS} and $E_{NS-25^{o}}$ and E_{EW} and $E_{EW-25^{o}}$ are approximately 10 and 19 percent respectively.

Power spectra both for measurements in the principal coordinate system and for measurements in the offset system rotated to the principal system for short periods are shown in figure 13. The power spectra for long-period telluric and magnetic data are given in figure 14. It can be seen that as far as the general forms of the curves are concerned, the rotated offset system results agree well with the principal system results for the E_{NS} component for both period ranges. For the E_{EW} component, the agreement is fairly good for the short-period data while for the long-period data it deteriorates with decreasing period. Also closer inspection of the telluric traces in figures 10 and 11 reveals that both for long and short-period cases the variations with periods at the beginning of each period band are present in both traces while the variations at shorter periods

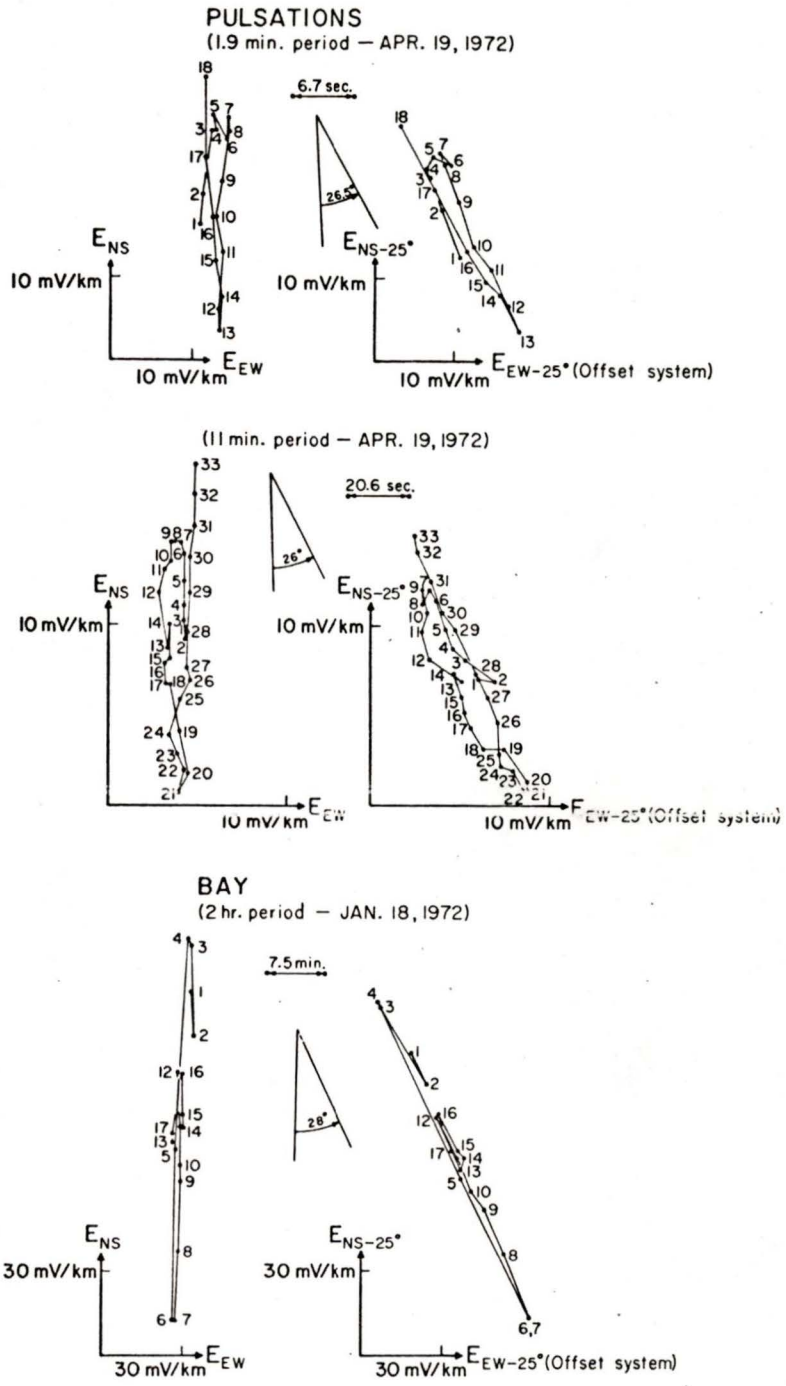

Figure 12. Polarization diagrams for the two telluric systems at Victoria.

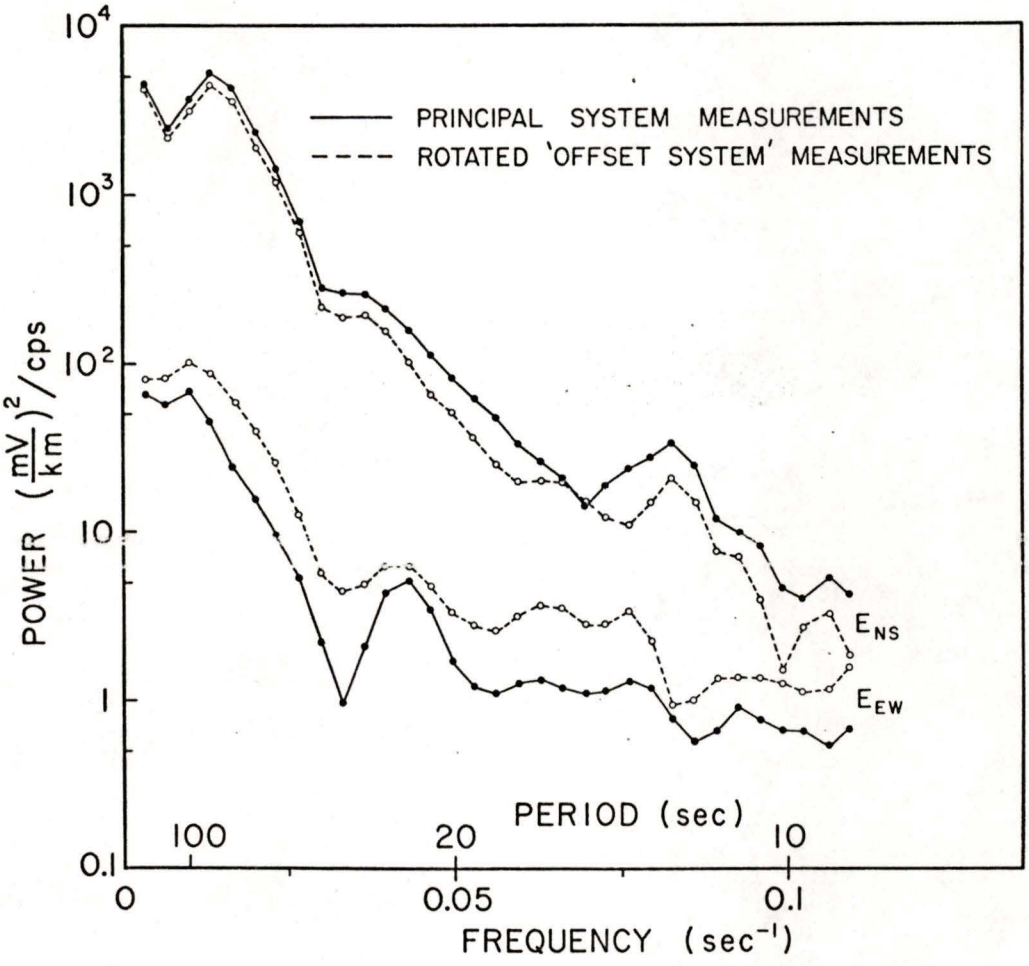

Figure 13. Power spectra for a short-period event (Apr. 19, 1972)

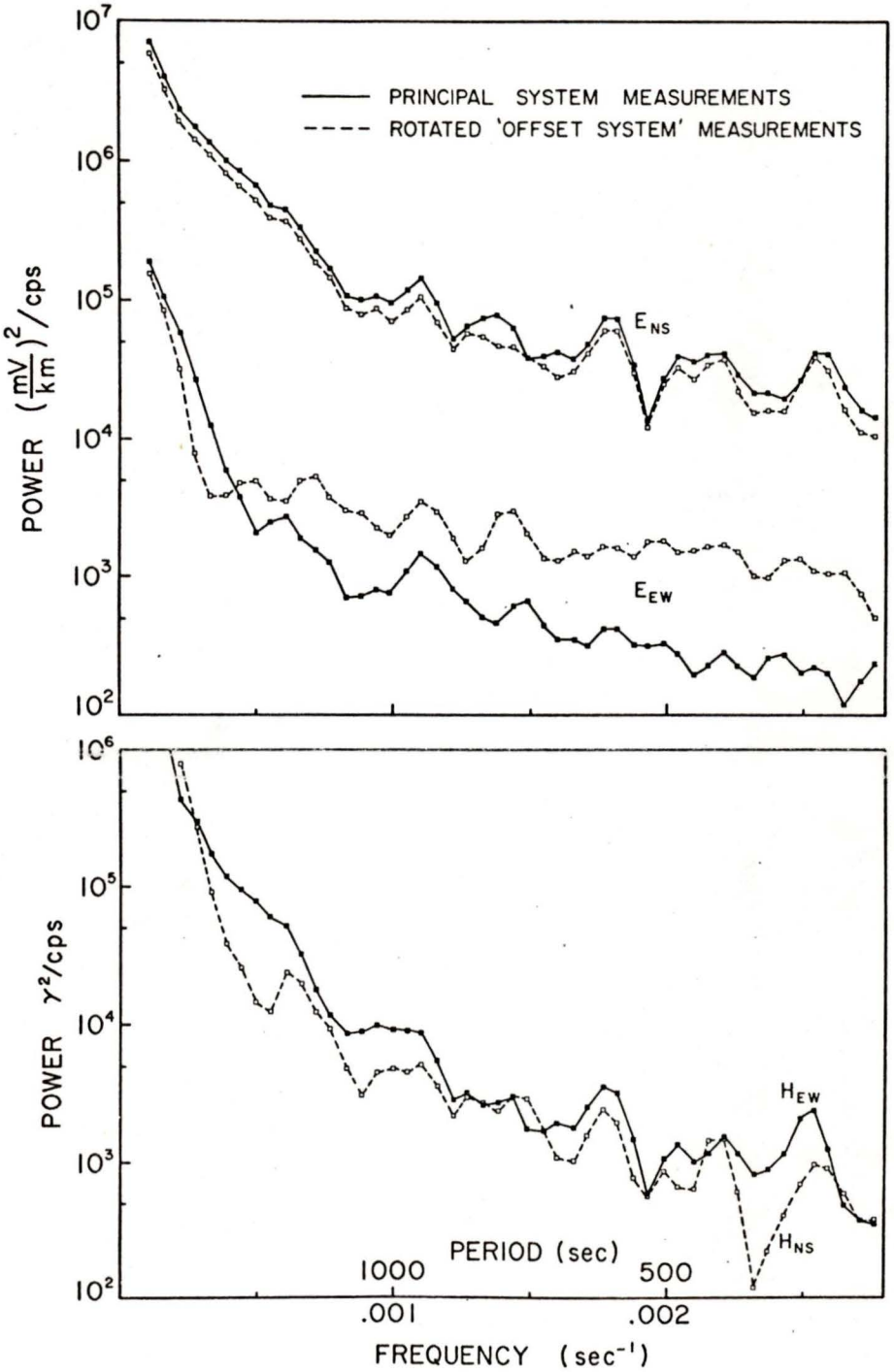

Figure 14. Power spectra for a long-period event (Jan. 16, 1972)

have a tendency to appear in the computationally rotated traces only. The low correlation at the shorter periods is probably due to the low resolution on the telluric strip chart traces since variations at shorter periods in both period bands occupy less chart space. An examination of the amplitude differences in $\underline{E}$ determined from the polarization plots for the principal and computationally rotated traces supports such a conclusion. For periods of two hours (near the beginning of the long-period band) and 2 minutes (near the beginning of the short-period band) the relative differences in $|E_{NS}|^2$ and $|E_{EW}|^2$ determined from the polarization plots in figure 12 are of approximately the same order. Similar values were obtained from the power spectra. However, for an intermediate, 11 minute period variation, the polarization plot in figure 11 (constructed from short-period band data) showed only a difference of 29% in $|E_{EW}|^2$ while the long-period power spectrum revealed a discrepancy of 75%. Such an observation is expected if a variation with an 11 minute period can be observed with greater resolution in the short-period band than the long-period band. The fact that the effect is more prominent for the EW case, where the level of signals is rather low, than the NS case, suggests that a low signal-to-noise ratio may also contribute to the poor correlation.

Another important observation concerning the power spectra is that for E_{NS} the computationally rotated spectrum is consistently lower than the spectrum of the principal system measurements while for E_{EW} the computationally rotated spectrum is consistently higher. A separation of the signal amplitudes into signal and noise parts in the rotation equations

shows that for the E_{NS} component noise is decreased by rotation while for the E_{EW} component it is increased. Thus, if noise were included as a possible explanation of the discrepancy between each pair of curves, it would explain the general trend of the separation. A signal-to-noise ratio of approximately 6:1 would explain the magnitude of the separation.

It is also possible that the measured fields are distorted by some small scale anomaly in the area of measurement. The telluric polarization and the differences in the E- and H-polarization apparent resistivity curves have demonstrated the existence of some anisotropy, either a continuous lateral inhomogeneity or a conductive interface. If the dimensions of the feature are large compared with the dimensions of the electrode array the rotation equations should be applicable. On the other hand, if the surface conductivity varies appreciably over a distance comparable to the electrode separation the fields may be distorted in such a way that they no longer transform as simple vectors.

CHAPTER 5

CONCLUSIONS

Magnetotelluric measurements at Victoria indicate polarization of the electric field measurements with the electric field in approximately the magnetic NS direction enhanced by a factor of 4 or more. The effect may be due to a high conducting surface feature with a conductive interface aligned approximately with the EW direction. Surface features of this nature near Victoria include a seawater channel and the Leech River fault. The conductivity contrast provided by the seawater channel is sufficiently high ($\sim 10^4$) to produce a strong effect but the irregular nature of the coastline makes a determination of the effective direction of the interface difficult. The conductivity contrast at the Leech River fault is considerably less (~ 10) than at the coast but the direction of the fault, if it extends across the Strait of Juan de Fuca, is approximately in the EW direction, perpendicular to the direction of the observed electric enhancement.

The data at Victoria have been interpreted in terms of a one dimensional model of the subsurface structure. The model proposes a highly resistive surface layer (~ 4000 Ωm) approximately 10 km thick over a highly conducting 10 km thick layer of approximately 9 Ωm resistivity. Below this, another highly resistive layer (~ 1000Ωm) extends into the earth's upper mantle. The results are in agreement with previous results for the "low Z" region of British Columbia determined by Caner (1971).

Both apparent resistivity curves (major and minor axes curves) can be combined into one interpretation to obtain realistic values for the conductivity structure. The present work demonstrates such a method and its advantages. The technique of constructing the minor axis apparent resistivity curve parallel to the major axis curve in the very short period range greatly improves the values for the resistivity and thickness of the first layer. The technique also takes advantage of the better quality of the major axis data.

Telluric measurements at Victoria only partially verify the form of the rotational transformation equations used in analyzing magnetotelluric data in anisotropic situations. A high, although perhaps not unreasonable, amount of noise could explain the observed discrepancies in the power spectral results. The discrepancies may also be due to a variation in surface conductivity in the region of measurement.

It may be useful to perform a more detailed investigation of the transformation for telluric measurements. If the conductivity is a tensor rather than a scalar quantity it should be possible to determine the components of this tensor (Reddy et al., 1972). The equations may be rewritten to accommodate the conductivity tensor and tested experimentally in a manner similar to the test of the simple rotation in the present work.

Mathematical support for the technique of improving the interpretation of magnetotelluric data using both E- and H-polarization apparent resistivity curves is also desirable. The technique was born from observations of theoretically calculated curves. A rigorous mathematical proof

that the electric field or at least the apparent resistivity for H-polarization measurements near the strike of a highly conducting body is uniformly enhanced in the short-period range would provide more confidence in the method.

A study of the effect of branch currents in the channel at Victoria using an analogue electromagnetic model similar to that of Dosso (1966) is of interest. Such an experiment could verify the existence of these branch currents as well as indicate the direction of telluric polarization produced by them at Victoria.

REFERENCES

Blackman, R.B. and Tukey, J.W. 1958. The Measurement of Power Spectra. Dover Publications, New York.

Cagniard, L. 1953. Basic theory of the magnetotelluric method of geophysical prospecting. Geophysics, 8, 605.

Caner, B. 1971. Quantitative interpretation of geomagnetic depth-sounding data in Western Canada. J. Geophys. Res., 76, 7202.

Caner, B. and Auld, D.R. 1968. Magnetotelluric determination of upper mantle conductivity structure at Victoria, British Columbia. Can. J. Earth Sci., 5, 1209.

Caner, B., Camfield, P.A., Anderson F., and Niblett, E.R. 1969. A large-scale magnetotelluric survey in Western Canada. Can. J. Earth Sci., 6, 1245.

Cantwell, T. and Madden, T.R. 1960. Preliminary report on crustal magnetotelluric measurements. J. Geophys. Res., 65, 4202.

Cochrane, N.A. and Hyndman, R.D. 1970. A new analysis of geomagnetic depth-sounding data from Western Canada. Can. J. Earth Sci., 7, 1208.

Crane, K.C.A. and Mainstone, J.S. 1972. Results of a comparison between a magnetotelluric model and micropulsation field observations. J. Geomag. Geoelec., 24, 91.

Davey, G.H. and Rosser, W.G.V. 1971. Effect of a coastline on the electric fields of geomagnetic micropulsations. J. Atmos. Terr. Phys., 33, 1823.

Dosso, W.H. 1966. Analogue model measurements for electromagnetic variations near a coastline. Can. J. Earth Sci., 3, 917.

Edwards, R.N., Law, L.K., and White, A. 1971. Geomagnetic variations in the British Isles and their relationship to electrical currents in the ocean and shallow seas. Phil. Trans. Roy. Soc., 270, 289.

Hibbs, R.D. and Jones, F.W. 1972. Apparent resistivity calculations for laterally inhomogeneous structures. Phys. Earth Planet. Interiors, 5, 184.

Lipskaya, N.V. 1953. On certain relationships between harmonics of the periodic variations of the terrestrial electric and magnetic fields. Izv. Akad. Nauk, USSR, Geophys. Series No. 1, 41.

Muller, J.E. 1971. Geological reconnaissance map of Vancouver Island and Gulf Islands. Open File Map, Geol. Surv. Can.

Niblett, E.R. and Sayn-Wittgenstein, C. 1960. Variation of electrical conductivity with depth by the magneto-telluric method. Geophysics, 25, 998.

Praus, O., DeLaurier, J.M., and Law, L.K. 1971. The extension of the Alert geomagnetic anomally through Northern Ellesmere Island, Canada. Can. J. Earth Sci., 8, 50.

Price, A.T. 1950. Electromagnetic induction in a semi-infinite conductor with a plane boundary. Quart. J. Mech. and Appl. Math., 3, 385.

Price, A.T. 1962. The Theory of magnetotelluric methods when the source field is considered. J. Geophys. Res., 67, 1907.

Rankin, D. and Reddy, I.K. 1970. Polarization of the magneto-telluric fields over an anisotropic earth. Pure and Applied Geophysics, 78, 58.

Reddy, I.K. and Rankin , D. 1972. On the interpretation of magnetotelluric data in the plains of Alberta. Can. J. Earth Sci., 9, 514.

Samson, J.C. 1969. Deep resistivity measurements in the Fraser Valley, British Columbia. Can. J. Earth Sci., 6, 1130.

Srivastava, S.P. 1963. Application of the magnetotelluric method to anisotropic and inhomogeneous bodies. J. Geophys. Res., 68, 5857.

Srivastava, S.P. 1965. Method of interpretation of magnetotelluric data when the source field is considered. J. Geophys. Res., 70, 945.

Srivastava, S.P. 1967. Magnetotelluric two- and three-layer master curves. Publ. Dom. Obs., Ottawa, 35, 309.

Srivastava, S.P. and White, A. 1971. Inland, coastal, and offshore magnetotelluric measurements in Eastern Canada. Can. J. Earth Sci., 8, 204.

Swift, C.M. 1967. A Magnetotelluric Investigation of an Electrical Conductivity Anomaly in the South-western United States. Ph.D. Dissertation, Massachusetts Institute of Technology, Cambridge, Massachusetts.

Tikhonov, A.N. 1950. Determination of the electrical characteristics of the deep strate of the earth's crust. Dok. Akad. Nauk, USSR, 73, 295.

Tikhonov, A.N. and Lipskaya, N.V. 1952. Terrestrial electric field variations. Dok. Akad. Nauk, 87, 547.

Trigg, D.F., Serson, P.H., and Camfield, P.A. 1971. A solid-state electrical recording magnetometer. Publ. Earth Phys. Branch, Ottawa, no.41.

Vozoff, K. 1972. The magnetotelluric method in the exploration of sedimentary basins. Geophysics, 37, 98.

Wait, J.R. 1954. On the relation between telluric currents and the earth's magnetic field. Geophysics, 19, 281.

Weaver, J.T. 1963. The electromagnetic field within a discontinuous conductor with reference to geomagnetic micropulsations near a coastline. Can. J. Phys., 41, 484.

Wescott, E.M. 1967. Coastal effects in magnetic and telluric current variations near a complex land, shelving seawater boundary. J. Geophys. Res., 72, 1959.

Wright, J.A. 1970. Anisotropic apparent resistivities arising from non-homogeneous two-dimensional structures. Can. J. Earth Sci., 7, 527.

APPENDIX A

COMPUTER PROGRAM LISTINGS

A.1 SPECT3

SPECT3 (obtained from E.M.R., Earth Physics Branch) carries out power spectral analysis on an orthogonal set of electric and magnetic field data simultaneously using statistical techniques (Blackman and Tukey, 1958). The program accepts a maximum of 2500 evenly spaced points of an E or H data series. An important feature of this program is the determination of auto and cross-correlations of the data and estimation of the coherence between magnetic and telluric signals. Auto-covariance of each series and the coherence of both series are given in the output along with power spectral estimates, apparent resistivities, and phase differences between the two series.

```
C     SPECT3  -  B. CANER                                                SP3 001
C     SPECT3.     THIS PROGRAM IS AN UPDATE (MAY 1970) OF SPECT2, TO
C       ELIMINATE THE FACTOR 3.14 IN POWER SPECTRAL OUTPUT. MODIFIED
C       CARDS ARE IDENTIFIED BY THE DIGIT 3 (INSTEAD OF 2) IN COLUMN 76.
C     FORTRAN IV. NOTE = THIS SOURCE DECK IS PUNCHED IN EBCDIC.          SP2 002
C     POWER SPECTRA WITH PREWHITENING, ADAPTED FOR MAGNETO-TELLURICS     SP2 003
C     TESTED AT UVIC ON IBM SYSTEM/360 MODEL 44,   MARCH 1970            SP2 004
C     CPU TIME WITH OBJECT DECK IS  65 SECS FOR 2 SERIES WITH 2000 DATA  SP2 005
C       POINTS EACH AND 100 ESTIMATES.                                   SP2 006
C     CPU TIME IS ROUGHLY PROPORTIONAL TO NDATA*NEST                     SP2 007
C     XS FIRST TIME SERIES (E-SERIES IN MAGNETO-TELLURICS)               SP2 008
C     YS SECOND TIME SERIES (H-SERIES IN MAGNETO-TELLURICS)              SP2 009
C     NDATA NUMBER OF DATA POINTS IN EACH SERIES                         SP2 010
C     NEST NUMBER OF ESTIMATES DESIRED                                   SP2 011
C     NFLAG = 0, ONE SERIES ONLY                                         SP2 012
C     NFLAG = 1, TWO SERIES                                              SP2 013
C     JFLAG = 0, PWR SPECTRA AND RATIO                                   SP2 014
C     JFLAG = 1, PWR SPECTRA AND MAGNETO-TELLURIC DATA (RHO)             SP2 015
C     DELT DIGITIZING INTERVAL IN SEC                                    SP2 016
C     MULT1 AND MULT2 ARE MULTIPLYING FACTORS FOR SERIES 1 AND 2. LEAVE  SP2 017
C        BLANK IF NOT REQUIRED.                                          SP2 018
C     PREW1 AND PREW2 ARE PREWHITENING FACTORS FOR SERIES 1 AND 2. LEAVE SP2 019
C        BLANK IF NOT REQUIRED. RECOLOURING IS PERFORMED ON OUTPUT DATA. SP2 020
C       NOTE THAT PREWHITENING MUST BE APPLIED TO BOTH SERIES, ALTHOUGH  SP2 021
C       THE PREWH. FACTOR NEED NOT BE THE SAME FOR BOTH SINCE RECOLOURED SP2 022
C       ESTIMATES ARE USED TO COMPUTE RHO OR RATIOS.                     SP2 023
C     IDEN1 AND IDEN2 SERIES IDENTIFICATION NUMBERS                      SP2 024
C                                                                        SP2 025
C     THIS PROGRAM IS LIMITED TO 300 ESTIMATES, 2500 POINTS EACH SERIES. SP2 026
      DIMENSION XX(301),YY(301),XMY(301), X(301),Y(301),                 SP2 027
     1YMX(301),XS(2501), YS(2501), A(301),B(301),C(301),D(301),XLAB(12), SP2 028
     2Z(301),W(301),PHI(301),XL(301),YL(301),R(301),OPC(301),T(301),     SP2 029
     3AOPC(301),BOPC(301),COPC(301),DOPC(301),RHO(301),OME(301)          SP2 030
      EQUIVALENCE (A,XX),(B,YY),(C,XM),(D,YM),(W,YMX),(Z,XMY)            SP2 031
      REAL MULT1,MULT2                                                   SP2 032
      DO 1000 KK=1,6
C                                                                        SP2 034
      READ(5,1) NDATA,NEST,NFLAG,JFLAG,DELT,MULT1,MULT2,PREW1,PREW2,     SP2 035
     1 IDEN1,IDEN2                                                       SP2 036
    1 FORMAT (4I5,3F10.3,2F5.2,10X,2I5)                                  SP2 037
      XNEST=FLOAT(NEST)                                                  SP2 038
      XNYP = DELT*2.0                                                    SP2 039
      XNYF = 1.0/XNYP                                                    SP2 040
      DF = XNYF/XNEST                                                    SP2 041
      NEST1=NEST+1                                                       SP2 042
      T(1) = 0.0                                                         SP2 043
      DO 180 I=2,NEST1                                                   SP2 044
  180 T(I) = 1.0/(DF*FLOAT(I-1))                                         SP2 045
      WRITE (6,100)                                                      SP2 046
      WRITE (6,600)                                                      SP2 047
      WRITE (6,700) IDEN1,IDEN2,DELT,NDATA,PREW1,PREW2,DF                SP2 048
  100 FORMAT (1H1)                                                       SP2 049
  600 FORMAT(53H T U K E Y  S P E C T R U M  E S T I M A T I O N  (3)//)   3 050
  700 FORMAT (5X8HSERIES  I5,2H /,I5,6X,5HDELT=F9.3,4H SEC,6X,8HNDATA =  SP2 051
     1I5,7H POINTS,6X,8H PREWH.=F5.2,1H/F5.2,6X,6HDELF= E11.4,4H CPS///) SP2 052
      READ (5,2)  (XS(I),I=1,NDATA)                                      SP2 053
    2 FORMAT (10F5.1,30X)
      IF(MULT1.EQ.0.0) GO TO 850                                         SP2 055
```

```
      DO 840 I=1,NDATA                                                  SP2 056
  840 XS(I) = XS(I)*MULT1                                               SP2 057
  850 SUMX = 0.0                                                        SP2 058
      DO 7 I=1,NDATA                                                    SP2 059
    7 SUMX = SUMX + XS(I)                                               SP2 060
      AVEX = SUMX/FLOAT(NDATA)                                          SP2 061
      DO 8 I = 1,NDATA                                                  SP2 062
    8 XS(I) = XS(I)-AVEX                                                SP2 063
      IF(PREW1.EQ.0.0) GO TO 44                                         SP2 064
      NDATA1 = NDATA - 1                                                SP2 065
      DO 4 I = 1,NDATA1                                                 SP2 066
      XS(I) = XS(I+1) - PREW1*XS(I)                                     SP2 067
    4 CONTINUE                                                          SP2 068
   44 CONTINUE                                                          SP2 069
      IF(NFLAG.EQ.1) GO TO 5                                            SP2 070
      IF(PREW1.NE.0.0).GO TO 14                                         SP2 071
      DO 3  I = 1,NDATA                                                 SP2 072
    3 YS(I) = XS(I)                                                     SP2 073
      GO TO 13                                                          SP2 074
   14 DO 15 I = 1,NDATA1                                                SP2 075
   15 YS(I) = XS(I)                                                     SP2 076
      NDATA = NDATA1                                                    SP2 077
      GO TO 13                                                          SP2 078
    5 READ (5,6) (YS(I), I=1,NDATA)                                     SP2 079
    6 FORMAT (10F5.1,30X)
      IF(MULT2.EQ.0.0) GO TO 870                                        SP2 081
      DO 860 I=1,NDATA                                                  SP2 082
  860 YS(I) = YS(I)*MULT2                                               SP2 083
  870 SUMY = 0.0                                                        SP2 084
      DO 9 I =1,NDATA                                                   SP2 085
    9 SUMY = SUMY + YS(I)                                               SP2 086
      AVEY = SUMY/FLOAT(NDATA)                                          SP2 087
      DO 11 I=1,NDATA                                                   SP2 088
   11 YS(I) = YS(I)-AVEY                                                SP2 089
      IF(PREW1.EQ.0.0) GO TO 13                                         SP2 090
      DO 16 I = 1,NDATA1                                                SP2 091
   16 YS(I)= YS(I+1) - PREW2*YS(I)                                      SP2 092
      NDATA = NDATA1                                                    SP2 093
C     FROM HERE ON NDATA IS ORIGINAL NDATA - 1 IF PREW. IS APPLIED      SP2 094
   13 CONTINUE                                                          SP2 095
      IF (NFLAG.EQ.0) GO TO 20                                          SP2 096
      DO 10 L=1,NEST1                                                   SP2 097
      YY(L)=0.0                                                         SP2 098
      XMY(L)=0.0                                                        SP2 099
      YMX(L)=0.0                                                        SP2 100
      DO 10 I=L,NDATA                                                   SP2 101
      LI=I-L+1                                                          SP2 102
      YY(L)=YY(L)+YS(LI)*YS(I)                                          SP2 103
      XMY(L)=XMY(L)+XS(LI)*YS(I)                                        SP2 104
   10 YMX(L)=YMX(L)+XS(I)*YS(LI)                                        SP2 105
C     AUTOCORRELATION SPECTRUM IS COMPUTED STARTING HERE.............. SP2 106
   20 DO 30 L=1,NEST1                                                   SP2 107
      XX(L)=0.0                                                         SP2 108
      DO 30 I=L,NDATA                                                   SP2 109
      LI=I-L+1                                                          SP2 110
   30 XX(L)=XX(L)+XS(I)*XS(LI)                                          SP2 111
      DO 40 L=1,NEST1                                                   SP2 112
      XD=FLOAT(NDATA-L+1)                                               SP2 113
```

```
   40 A(L)=XX(L)/XD                                                    SP2 114
      DO 51 L=2,NEST                                                   SP2 115
      M = L-1                                                          SP2 116
      XM = FLOAT(M)                                                    SP2 117
      XM = 3.14159265/XNEST*XM                                         SP2 118
      OPC(L) = 1.0 + COS(XM)                                           SP2 119
   51 AOPC(L)=OPC(L)*A(L)                                              SP2 120
      IF (NFLAG.EQ.0) GO TO 150                                        SP2 121
      DO 50 L=1,NEST1                                                  SP2 122
      XD=FLOAT(NDATA-L+1)                                              SP2 123
      B(L)=YY(L)/XD                                                    SP2 124
      C(L)=XMY(L)/XD                                                   SP2 125
   50 D(L)=YMX(L)/XD                                                   SP2 126
      DO 52 L=2,NEST                                                   SP2 127
      BOPC(L)=OPC(L)*B(L)                                              SP2 128
      COPC(L)=OPC(L)*(D(L)-C(L))                                       SP2 129
   52 DOPC(L)=OPC(L)*(D(L)+C(L))                                       SP2 130
      DO 60 K=1,NEST1                                                  SP2 131
      Y(K)=0.0                                                         SP2 132
      Z(K)=0.0                                                         SP2 133
      W(K)=0.0                                                         SP2 134
      DO 55 L=2,NEST                                                   SP2 135
      CS=3.14159265/XNEST*FLOAT((K-1)*(L-1))                           SP2 136
      CS1=COS(CS)                                                      SP2 137
      Y(K)=Y(K)+CS1*BOPC(L)                                            SP2 138
      Z(K)=Z(K)+0.5*CS1*DOPC(L)                                        SP2 139
   55 W(K)=W(K)+0.5*SIN(CS)*COPC(L)                                    SP2 140
      Y(K)=(Y(K)+B(1))*(DELT*3.14159265)                                 3 141
      Z(K)=(Z(K)+C(1))*(DELT*3.14159265)                                 3 142
   60 W(K)=W(K)*(DELT*3.14159265)                                        3 143
      Y(1)=0.5*Y(1)*DELT                                               SP2 144
      Z(1)=0.5*Z(1)*DELT                                               SP2 145
      Y(NEST1)=0.5*Y(NEST1)*DELT                                       SP2 146
      Z(NEST1)=0.5*Z(NEST1)*DELT                                       SP2 147
      W(1)=0.5*W(1)                                                    SP2 148
      W(NEST1)=0.5*W(NEST1)                                            SP2 149
      IF(PREW1.NE.0.0) GO TO 131                                       SP2 150
C     IF PREWHITENING IS APPLIED, LOG IS NOT COMPUTED                  SP2 151
      DO 130 L=1,NEST1                                                 SP2 152
      IF(Y(L).LT..00001) GO TO 129                                     SP2 153
      YL(L)=ALOG10(Y(L))+10.                                           SP2 154
      GO TO 130                                                        SP2 155
  129 YL(L)=0.0                                                        SP2 156
  130 CONTINUE                                                         SP2 157
  131 CONTINUE                                                         SP2 158
  150 DO 160 K=1,NEST1                                                 SP2 159
      X(K)=0.0                                                         SP2 160
      DO 155 L=2,NEST                                                  SP2 161
      CD = 3.14159265/XNEST*FLOAT((K-1)*(L-1))                         SP2 162
      CD1 = COS(CD)                                                    SP2 163
  155 X(K) = X(K)+CD1*AOPC(L)                                          SP2 164
  160 X(K)=(X(K)+A(1))*(DELT*3.14159265)                                 3 165
      X(1)=0.5*X(1)*DELT                                               SP2 166
      X(NEST1)=0.5*X(NEST1)*DELT                                       SP2 167
      IF(PREW1.NE.0.0) GO TO 171                                       SP2 168
C     IF PREWHITENING IS APPLIED, LOG IS NOT COMPUTED                  SP2 169
      DO 170 L=1,NEST1                                                 SP2 170
      IF (X(L).LT..00001) GO TO 169                                    SP2 171
```

```
      XL(L)=ALOG10(X(L))+10.                                          SP2 172
      GO TO 170                                                       SP2 173
  169 XL(L)=0.0                                                       SP2 174
  170 CONTINUE                                                        SP2 175
  171 CONTINUE                                                        SP2 176
      IF(NFLAG.EQ.0) GO TO 500                                        SP2 177
      DO 200 L=1,NEST1                                                SP2 178
      R(L) = (Z(L)**2+W(L)**2)/(X(L)*Y(L))                            SP2 179
      R(L) =SQRT(ABS(R(L)))                                           SP2 180
  200 PHI(L) = -1.0*ATAN2 (W(L),Z(L))*57.2957786                      SP2 181
      IF(PREW1.EQ.0.0) GO TO 201                                      SP2 182
C     FROM HERE TO 114 APPLIES ONLY IF PREWHITENED                    SP2 183
      DO 231 L=1,NEST1                                                SP2 184
      OME(L) = (3.14159*FLOAT(L-1))/XNEST                             SP2 185
      OME(L) = COS(OME(L))                                            SP2 186
      XL(L) = (X(L))/(1.0+PREW1*PREW1-2.0*PREW1*OME(L))               SP2 187
      YL(L) = (Y(L))/(1.0+PREW2*PREW2-2.0*PREW2*OME(L))               SP2 188
  231 CONTINUE                                                        SP2 189
      IF(JFLAG.EQ.0) GO TO 301                                        SP2 190
      DO 232 L=1,NEST1                                                SP2 191
      RHO(L) = XL(L)/YL(L)                                            SP2 192
  232 RHO(L) = 0.2*RHO(L)*T(L)                                        SP2 193
      WRITE (6,213)                                                   SP2 194
      WRITE (6,223)                                                   SP2 195
  213 FORMAT (3X1HK,4X4HA(K),7X4HE(K),10X4HE(K),9X4HB(K),9X4HH(K),    SP2 196
     18X4HH(K),9X4HR(K),6X6HPHI(K),5X7HT(K)SEC,5X6HRHO(K))            SP2 197
  223 FORMAT (19X,8HPREWHITE,3X10HRECOLOURED,17X8HPREWHITE,           SP2 198
     14X10HRECOLOURED//)                                             SP2 199
      GO TO 401                                                       SP2 200
  301 DO 351 L=1,NEST1                                                SP2 201
  351 RHO(L) = XL(L)/YL(L)                                            SP2 202
      WRITE (6,113)                                                   SP2 203
      WRITE (6,123)                                                   SP2 204
  113 FORMAT (3X1HK,4X4HA(K),7X4HX(K),10X4HX(K),9X4HB(K),9X4HY(K),    SP2 205
     18X4HY(K),9X4HR(K),6X6HPHI(K),5X7HT(K)SEC,5X9HX(K)/Y(K))         SP2 206
  123 FORMAT (19X,8HPREWHITE,3X10HRECOLOURED,17X8HPREWHITE,           SP2 207
     14X10HRECOLOURED//)                                             SP2 208
  401 DO 251 I=1,NEST1                                                SP2 209
      L = I-1                                                         SP2 210
  251 WRITE (6,114) L,A(I),X(I),XL(I),B(I),Y(I),YL(I),R(I),PHI(I),T(I), SP2 211
     1RHO(I)                                                          SP2 212
  114 FORMAT (1H0,I4,E11.3,2E12.3,2X,E11.3,2E12.3,2X,2(F9.3,2X),2E12.3) SP2 213
      GO TO 999                                                       SP2 214
  201 IF(JFLAG.EQ.0) GO TO 300                                        SP2 215
      DO 230 L=1,NEST1                                                SP2 216
      RHO(L) = X(L)/Y(L)                                              SP2 217
  230 RHO(L) = 0.2*RHO(L)*T(L)                                        SP2 218
      WRITE (6,203)                                                   SP2 219
  203 FORMAT (3X1HK,4X4HA(K),9X4HE(K),8X7HLOGE+10,7X4HB(K),9X4HH(K),  SP2 220
     16X7HLOGH+10,5X4HR(K),6X6HPHI(K),5X7HT(K)SEC,5X6HRHO(K)//)       SP2 221
      GO TO 400                                                       SP2 222
  300 DO 350 L=1,NEST1                                                SP2 223
  350 RHO(L) = X(L)/Y(L)                                              SP2 224
      WRITE (6,103)                                                   SP2 225
  103 FORMAT (3X1HK,4X4HA(K),9X4HX(K),8X7HLOGX+10,7X4HB(K),9X4HY(K),  SP2 226
     16X7HLOGY+10,5X4HR(K),6X6HPHI(K),5X7HT(K)SEC,5X9HX(K)/Y(K)//)    SP2 227
  400  DO 250 I=1,NEST1                                               SP2 228
      L=I-1                                                           SP2 229
```

```
  250 WRITE (6,104) L,A(I),X(I),XL(I),B(I),Y(I),YL(I),R(I),PHI(I),T(I),   SP2 230
     1 RHO(I)                                                             SP2 231
  104 FORMAT (1H0,I4,2E13.4,F9.3,2X2E13.4,3(F9.3,2X),2E12.3)              SP2 232
      GO TO 999                                                           SP2 233
  500 IF(PREW1.EQ.0.0) GO TO 501                                          SP2 234
C     FROM HERE TO 116 APPLIES ONLY IF PREWHITENED                        SP2 235
      WRITE (6,115)                                                       SP2 236
      WRITE (6,125)                                                       SP2 237
  115 FORMAT (9X1HK,5X4HA(K),11X4HX(K),11X4HX(K),7X7HT(K)SEC)             SP2 238
  125 FORMAT(28X,8HPREWHITE,4X,10HRECOLOURED//)                           SP2 239
      DO 511 I=1,NEST1                                                    SP2 240
      OME(I) = (3.14159*FLOAT(I-1))/(XNEST*DELT)                          SP2 241
      CME(I) = COS(OME(I))                                                SP2 242
      XL(I) = (X(I))/(1.0+PREW1*PREW1-2.0*PREW1*OME(I))                   SP2 243
      L = I-1                                                             SP2 244
  511 WRITE (6,116) L,A(I),X(I),XL(I),T(I)                                SP2 245
  116 FORMAT (1H0,I10,3E13.4,E12.3)                                       SP2 246
      GO TO 999                                                           SP2 247
  501 WRITE (6,105)                                                       SP2 248
  105 FORMAT (9X1HK,5X4HA(K),11X4HX(K),10X7HLOGX+10,7X7HT(K)SEC//)        SP2 249
  106 FORMAT (1H0,I10,2E15.6,F10.3,E12.3)                                 SP2 250
      DO 510 I=1,NEST1                                                    SP2 251
      L=I-1                                                               SP2 252
  510 WRITE (6,106) L,A(I),X(I),XL(I),T(I)                                SP2 253
C     OUTPUT PARAMETERS =                                                 SP2 254
C     A(K) AND B(K) AUTOCOVARIANCE OF X (OR E) AND Y (OR H) SERIES        SP2 255
C     E(K) AND H(K) ARE POWER SPECTRAL ESTIMATES.                          3 256
C     PWR.SP.EST. = ((A**2)/2)/DELF                  (A=FOURIER AMPL.)    SP2 257
C     LOGH AND LOGY ARE LOG10 OF PWR.SP.ESTIMATES PLUS 10.0               SP2 258
C     IF PREWHITENING IS APPLIED, LOGS ARE NOT COMPUTED                   SP2 259
C     R(K) COHERENCE OF SERIES 1 AND 2                                    SP2 260
C     PHI IS PHASE DIFFERENCE, SERIES 1 LEADING OVER SERIES 2             SP2 261
C     T(K) PERIOD IN SECS                                                 SP2 262
C     RHO(K) APPARENT RESISTIVITY IN OHM-METERS                           SP2 263
C                                                                         SP2 264
  999 CONTINUE                                                            SP2 265
 1000 CONTINUE                                                            SP2 266
      STOP                                                                SP2 267
      END                                                                 SP2 268
```

A.2 MT3LAY

MT3LAY (obtained from E.M.R., Earth Physics Branch) calculates the values of apparent resistivity at the surface of a three-layered medium at any given periods. For input data, the program accepts any number of values for the source parameter and thicknesses of the first two layers provided that the number of values in each case is specified on the first data card. On the other hand, only three values are permitted for the resistivity of each of the three layers. The models are those resulting from a one-to-one correspondence between the groups of values rather than all possible permutations. The program in its present form is capable of calculating apparent resistivities at 16 points in the period domain which are entered as input data. However, the number and spacing of these can easily be changed by changing the appropriate read statement and the two DO statements involving the integer K.

```
C       MT3LAY  -  B.CANER
C       THREE-LAYER CONDUCTIVITY STRUCTURE MODELS FOR MAGNETO-TELLURICS
C       TESTED ON UVIC SYSTEM 360 /MODEL 44, AUGUST 1967
C       TIME 4.5 MIN FOR NH1*NH2*NV=45. INCLUDING 0.7 MIN FOR COMPILE
        DIMENSION P(32),V(5),H2(5),R(3,3),E(3,3),B(3,3),C(3,3),RA(3),
       1THETA(3),H1(5),T(32),RO(3)
        READ (5,6) NH1,NH2,NV
        READ (5,7) (H1(N),N=1,NH1)
        READ (5,7) (H2(M),M=1,NH2)
        READ (5,8) (V(L) ,L=1,NV)
        READ (5,9) ((R(I,J),J=1,3),I=1,3)
        READ (5,10) (P(K),K=1,16)
    6 FORMAT (3I5)
    7 FORMAT (5F10.2)
    8 FORMAT (5F10.4)
    9 FORMAT (9F8.1)
   10 FORMAT (8F10.1)
C       NH1,NH2,NV  ARE NUMBERS OF CASES TO BE RUN, UP TO 5 FOR EACH.
C       H1 IS THICKNESS OF TOP LAYER IN KM
C       H2 IS THICKNESS OF MIDDLE LAYER IN KM
C       V IS SPATIAL WAVE-NUMBER ,IN KM-1
C       R ARE RESISTIVITIES IN OHM-METERS,ENTERED IN FOLLOWING ORDER-
C       TOP LAYER CASE 1, TOP CASE 2, TOP CASE 3, MID LAYER CASE 1,
C       MID CASE 2, MID CASE 3, BOTTOM CASE 1, BOT. CASE 2,BOT.CASE3.
C       P(K) ARE PERIODS, IN SECONDS
        W2 = 0.70710678
        RADEG = 57.295783
C       FOLLOWING GROUP IS OVERALL PROBLEM HEADING (INPUT PARAMETERS)
        WRITE (6,100)
        WRITE (6,26)
   26 FORMAT (36H MAGNETO-TELLURIC THREE-LAYER MODELS//)
        WRITE (6,102)
        WRITE (6,27)
   27 FORMAT (18H INPUT PARAMETERS=//)
        DO 13 N=1,NH1
   13 WRITE (6,23) H1(N)
        WRITE (6,102)
        DO 14 M=1,NH2
   14 WRITE (6,24) H2(M)
        WRITE (6,102)
        DO 15 L=1,NV
   15 WRITE (6,25) V(L)
   23 FORMAT (10X,9H H1(KM) =,F12.2)
   24 FORMAT (10X,9H H2(KM) =,F12.2)
   25 FORMAT (10X,9H V(KM-1)=,E11.3)
C
        DO 30 K=1,16
   30 T(K) = P(K)*10.0
        DO  60  N=1,NH1
        DO  60  M=1,NH2
        WRITE (6,100)
        WRITE (6,16) N,H1(N)
        WRITE (6,17) M,H2(M)
        WRITE (6,18) R(1,1),R(1,2),R(1,3)
        WRITE (6,19) R(2,1),R(2,2),R(2,3)
        WRITE (6,20) R(3,1),R(3,2),R(3,3)
        DO 60  L= 1,NV
        WRITE (6,102)
```

```
      WRITE (6,21) L,V(L)
      VL=V(L)
      VL2 = VL*VL
      VL4 = VL2*VL2
      DO 60  K= 1,16
      DO 40  I= 1,3
      DO 40  J= 1,3
      RIJ = R(I,J)
      TK  = T(K)
      A1  = 78.956835 /(RIJ*TK)
      E(I,J) = A1*A1
      A2 = SQRT(E(I,J)+VL4)
      B(I,J) = (SQRT(A2+VL2))*W2
   40 C(I,J) = (SQRT(ABS(A2-VL2)))*W2
      DO 50  J=1,3
      B1J = B(1,J)
      B2J = B(2,J)
      B3J = B(3,J)
      C1J = C(1,J)
      C2J = C(2,J)
      C3J = C(3,J)
      A3 = B2J*B2J+C2J*C2J
      A4 = B3J*B3J+C3J*C3J
      AA = (B1J*B2J+C1J*C2J)/A3
      BB = (B2J*C1J-B1J*C2J)/A3
      CC = (B2J*B3J+C2J*C3J)/A4
      DD = (B3J*C2J-B2J*C3J)/A4
      XH1 = B1J*H1(N)
      YH1 = C1J*H1(N)
      XH2 = B2J*H2(M)
      YH2 = C2J*H2(M)
      F1 = SIN(YH1)/COS(YH1)
      EX1 = EXP(+XH1)
      EX2 = EXP(-XH1)
      F2  = (EX1-EX2)/(EX1+EX2)
      F3  = SIN(YH2)/COS(YH2)
      EX1 = EXP(+XH2)
      EX2 = EXP(-XH2)
      F4 = (EX1-EX2)/(EX1+EX2)
      SS = F2*(1.0+F1*F1)
      TT = F1*(1.0-F2*F2)
      UU = 1.0+F1*F1*F2*F2
      PP = F4*(1.0+F3*F3)
      QQ = F3*(1.0-F4*F4)
      RR = 1.0+F4*F4*F3*F3
      F5 = SQRT(1.0+VL4/E(1,J))
      XX = AA*UU*(CC*RR+PP)-BB*UU*(DD*RR+QQ)+SS*RR+SS*(CC*PP-QQ*DD)-
     1TT*(PP*DD+CC*QQ)
      YY = AA*UU*(DD*RR+QQ)+BB*UU*(CC*RR+PP)+SS*(PP*DD+CC*QQ)+TT*RR+
     1TT*(CC*PP-QQ*DD)
      WW = UU*RR+UU*(CC*PP-QQ*DD)+(AA*SS-BB*TT)*(CC*RR+PP)-(BB*SS+AA*TT)
     1*(DD*RR+QQ)
      ZZ = UU*(PP*DD+CC*QQ)+(AA*SS-BB*TT)*(DD*RR+QQ)+(BB*SS+AA*TT)*
     1(CC*RR+PP)
      F6 = (WW*WW+ZZ*ZZ)*F5
      E15 = YY*(WW*C1J+B1J*ZZ)-XX*(ZZ*C1J-WW*B1J)
      E16 = XX*(WW*C1J+B1J*ZZ)+YY*(ZZ*C1J-WW*B1J)
      RA(J) = (XX*XX+YY*YY)/F6
```

```
      RO(J) = RA(J)*R(1,J)
      PH = ATAN(ABS(E15/E16))
      IF(E16)42,41,41
   41 IF(E15)45,43,43
   42 IF(E15)47,49,49
   43 THETA(J) = PH*RADEG
   44 GO TO 50
   45 THETA(J) = (6.28318-PH)*RADEG
   46 GO TO 50
   47 THETA(J) = (3.14159+PH)*RADEG
   48 GO TO 50
   49 THETA(J) = (3.14159-PH)*RADEG
   50 CONTINUE
   60 WRITE (6,22) K,P(K),RO(1),THETA(1),RO(2),THETA(2),RO(3),THETA(3)
   16 FORMAT (5H  H1(I1,3H) =F12.3,3H KM)
   17 FORMAT (5H  H2(I1,3H) =F12.3,3H KM)
   18 FORMAT (29X7HR(1,1)=E14.4,15X7HR(1,2)=E14.4,15X7HR(1,3)=E11.4)
   19 FORMAT (29X7HR(2,1)=E14.4,15X7HR(2,2)=E14.4,15X7HR(2,3)=E11.4)
   20 FORMAT (29X7HR(3,1)=E14.4,15X7HR(3,2)=E14.4,15X7HR(3,3)=E11.4)
   21 FORMAT (4H0 V(I1,3H) =E11.4,5H KM-1)
   22 FORMAT (3H P(I2,2H)=E10.3,5X4HRO1=E10.3,9H  THETA1=F7.2,5X4HRO2=
     1E10.3,9H  THETA2=F7.2,5X4HRO3=E10.3,9H  THETA3=F7.2)
  100 FORMAT (1H1)
  102 FORMAT (1H0)
  999 RETURN
C     OUTPUT PARAMETERS =
C     P(K) PERIODS IN SEC
C     RO APPARENT RESISTIVITIES IN OHM-METERS
C     THETA PHASE LEAD TELLURIC OVER MAGNETIC SERIES, IN DEGREES
      END
```

Surname: NIENABER Given Names: WILFRED

Place of Birth: WILHELMSHAVEN, GERMANY Date of Birth: June 19, 1947

Educational Institutions Attended, with Dates of Entering and Leaving:

UNIVERSITY OF VICTORIA 1965-1969

Degrees, Diplomas, Etc., Awarded, with Dates and Names of Institutions:

B.Sc. 1969 University of Victoria

Honors and Awards:

Publications:

Nienaber, W., Auld, D.R., and Dosso, H.W. 1973.

Analysis of anisotropic magnetotelluric measurements at Victoria, B.C. Can. J. Earth Sci., 10, 557.

PARTIAL COPYRIGHT LICENSE

I hereby grant the right to lend my thesis or dissertation (the title of which is shown below) to users of the University of Victoria Library, and to make single copies only for such users or in response to a request from the library of any other university, or similar institution, on its behalf or for one of its users. I further agree that permission for extensive copying of this thesis for scholarly purposes may be granted by me or a member of the University designated by me. It is understood that copying or publication of this thesis for financial gain shall not be allowed without my written permission.

Title of Thesis

A Magnetotelluric Study of

Southern Vancouver Island

Author [redacted]

Signature

WILFRED NIENABER

June 1973